OPTICAL FIBER BASED FLUORESCENCE ENDOMICROSCOPE WITH CELLULAR IMAGING

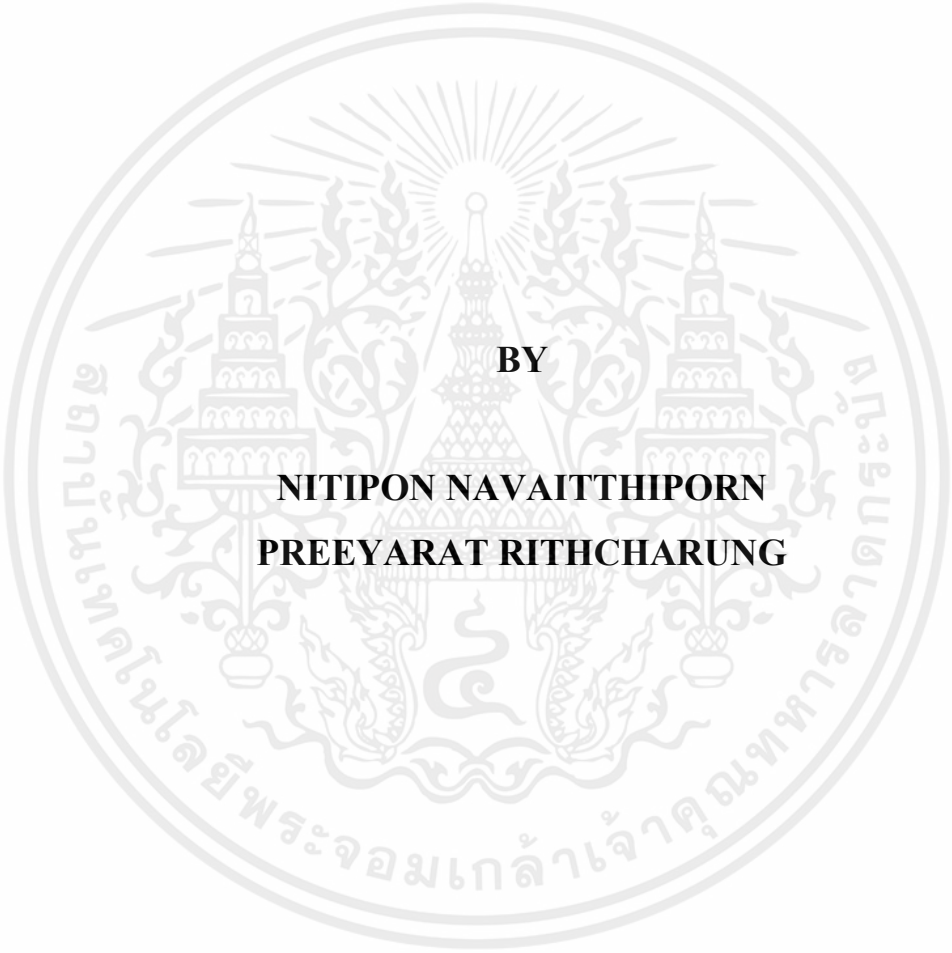

BY

NITIPON NAVAITTHIPORN

PREEYARAT RITHCHARUNG

A PROJECT SUBMITTED IN PARTIAL FULFILLMENT OF THE REQUIREMENTS FOR THE DEGREE OF BACHELOR OF ENGINEERING IN BACHELOR'S DEGREE

KING MONGKUT'S INSTITUTE OF TECHNOLOGY LADKRABANG

ACADEMIC YEAR 2020

FACULTY OF ENGINEERING

KING MONGKUT'S INSTITUTE OF TECHNOLOGY LADKRABANG

PROJECT CERTIFICATE

Project Title	Optical fiber based fluorescence endomicroscope with cellular imaging
Student Name	Mr. Nitipon Navaitthiporn Student ID. 60011243 Miss Preeyarat Rithcharung Student Student ID. 60011261
Degree	Bachelor of Engineering in Biomedical Engineering
Project Advisor	Signed: _____ (Dr. Wibool Piyawattanametha)
Committee	Signed: _____ (Assoc. Prof. Dr. Chuchart Pintavirooj)
	Signed: _____ (Assoc. Prof. Dr. Supan Tungjitkusolmun)
	Signed: _____ (Asst. Prof. Dr. Treesukon Treebupachatsakul)
Head of Department	Signed: _____ (Asst. Prof. Dr. Sarinporn Visitsattapongse)

Project Title	Optical fiber based fluorescence endomicroscope with cellular imaging
Student Name	Mr. Nitipon Navaitthiporn Miss Preeyarat Rithcharung
Degree	Bachelor of Engineering in Biomedical Engineering
Project Advisor	Dr.Wibool Piyawattanametha
Academic Years	2020

ABSTRACT

Cervical cancer is the second most common cancer in women worldwide. Early diagnosis is extremely important for successful treatments. The current primary screening method for cervical abnormal growth is PAP smear. It is labour intensive and time consuming with a significant number of false positives/negatives. In suburban and rural areas of Thailand, it takes 1-3 weeks for patients to get their PAP results. Mobile colposcope could be used as a co-test immediately after a PAP smear to reduce the false positive or negative results. However, experienced colposcopists are not always available. Hence, there is a need for an effective and real-time screening method that gives an early and confident diagnosis at low-resource settings of Thailand.

Therefore, in order to cope with the incidence of cervical cancer, Visual Inspection with Acetic acid screening has been developed to be used for primary screening of cervical cancer, which can significantly reduce the number of cervical cancer cases. Hence, the development of cervical cancer screening to be effective and able to reduce the number of cervical cancer cases can be done by increasing the potential for Visual Inspection (VI) testing to be accurate and specific to the joints. Cervical cancer in the early stages even more screening can be performed early in the pre-cancer stage, making the treatment easier and faster. This supports the single visit approach (SVA) to be more reliable in diagnostic results. By developing an endoscopic microscopy that supports multiple wavelengths and capable of capturing cellular resolution (5–10-micron range) images in combination with fluorescent labelled

peptides. FITC to show the location of the lesion at the cellular level. From the aforementioned theories, it leads to the following hypotheses. Multiwavelength and cellular resolution endoscopy microscopes can be using readily available equipment and improved image quality through software processing and able to develop techniques for screening cervical cancer in the early stages before cancer by using the camera developed in this project with a specific peptide capable of locating lesions.

ACKNOWLEDGEMENTS

First and foremost we are extremely grateful to our supervisor, Dr.Wibool Piyawattanametha for his invaluable advice, continuous support, motivation, enthusiasm, and patience during our Bachelor's degree study. His immense knowledge and plentiful experience have encouraged us in all the time of our academic research and daily life. We would also like to thank Asst.Prof.Dr. Treesukon Treebupachatsakul, Asst. Prof. Dr. Sarinporn Visitsattapongse and Mr. Nutthanan Wanluk for their technical support on our study. We would like to thank all the members in Biomedical Engineering, KMITL. It is their kind help and support that have made our study and life in the King Mongkut's Institute of Technology Ladkrabang a wonderful time. In addition, we would like to express our gratitude to our parents for their support. Without their tremendous understanding and encouragement in the past few years, it would be impossible for us to complete our study.

TABLE OF CONTENTS

LIST OF TABLES

LIST OF FIGURES

LIST OF SYMBOLS/ABBREVIATIONS

Symbols/Abbreviations	Terms
VIA	Visual inspection with acetic acid
VIAM	VIA with low-level magnification
VIVL	VI with Lugol's idodine
HPV	Human Papillomavirus
NIR	Near infrared
HRME	High resolution microendoscope
GUI	Graphical User Interface
FOV	Field of view
hrHPV	high-risk human papillomavirus
ASCCP	American Society for Colposcopy and Cervical Pathology
ACS	American Cancer Society
LEDs	light-emitting diodes
OD	Optical density
CWL	Central Wavelength
FWHM	Full width half maximum
FOE	Fiber Optical Endoscope

CHAPTER 1
INTRODUCTION

Since 2018, the fourth most common cancer in women is cervical cancer inferior to breast, colorectal, and lung cancers. In 2018, the case fatality rate of cervical cancer worldwide was 311,000 cases in women. Per 100,000 of population, cervical cancer incidence is 23 for Indonesia, 21 for Myanmar, 15 for Philippines, 18 for Thailand, 12 for Laos, 11 for Malaysia, and 8 for Vietnam [1].

Cervical cancer screening has depended on the conventional Pap smear method, a well-recognized method that is labor intensive, requires trained healthcare personnel, and possesses a high false negative/positive rate. Liquid-based cytology is more sensitive to detect cervical neoplasia compared to Pap smear. In contrast, the Pap smear test is more specific to detect cervical neoplasia compared to liquid-based cytology. Either visual inspection with acetic acid (VIA) or VIA with low-level magnification (VIAM) is case alight in terms of cost and effectiveness compared to a conventional pap smear. VI with Lugol's idodine (VILI) was re-evaluated and showed slight superior sensitivity compared to VIA. Human Papillomavirus (HPV) testing is now reliable, but it requires sophisticated laboratory infrastructure. Thus, it is a higher cost when compared to other cervical cancer screening methods [2]. Therefore, identification of new reliable technologies for early cervical detection is imperative.

Then, a noninvasive technique involving the use of light with varying wavelengths to diagnose the suspected tissues in vivo has been introduced. Endoscopes are optical instruments that suitable for macroscopic view inspection of the large mucosal surfaces in hollow organs internal to the human body such as the esophagus, colon, and cervix. For example, Later, Pierce et al. demonstrated the use of a low-cost fiber-optic microscope that can provide real-time imaging in cell culture, animals, and patients [3].

Nowadays, targeted molecular imaging of tumor growth has been emerging. Molecular imaging probes have assisted in understanding of fundamental biological processes. Tremendous progress has been made in both discovery of imaging probes and development of imaging instruments for assisting the development of tumor.

Currently, in vivo imaging could be applied at preclinical and clinical to improvements in optical systems, and imaging instruments. These technologies in a combination with optical imaging probes provide noninvasive, and real-time imaging at cellular levels. Indeed, the combination of these technologies has enhanced the performance of optical imaging systems [4].

1.1 Cervical cancer survival rate by stages

Cancer of cervix is caused by a virus called HPV (Human Papilloma Virus), a virus transmitted by sexual intercourse that causes skin abrasions and the virus to enter the cervix. This causes the cervix to have alterations of tissues or cells from the normal cervix to the pre-stage cervical cancer.

1.1.1 Stage I: The cancer has limited only to the cervix.

1.1.2 Stage II: The cancer spreads outside the cervix but does not reach the side walls of the pelvis.

1.1.3 Stage III: The cancer spreads to the side walls of the pelvis.

1.1.4 Stage IVA: The cancer spreads outside the pelvis or spreads to the bladder lining or rectum.

1.1.5 Stage IVB: The cancer has already spread throughout other organ in the body [5].

1.2 Cervical cancer statistic

Cervical cancer is most often diagnosed in women around the ages of 35 and 44. There are 20% of cervical cancers are diagnosed in women over age 65. Usually, those cases occur in women who did not receive yearly cervical cancer screenings before age 65. The 5-year survival rate for all women that being cervical cancer is 66%. However, survival rates could vary by many factors such as age, immunity of each person, race. Survival rates depend on many factors, including diagnosis of cervical cancer. Whenever detected at an early stage, the 5-year survival rate for women with invasive cervical cancer is 92%. There are only 44% of women with cervical cancer are diagnosed at an early stage. If cervical cancer has spread to other organs or lymph nodes, the 5-year survival rate is 56%. If cancer has spread to a distant part of the body, the 5-year survival rate is 17% [6].

1.3 Importance of early detection

Screening could assist to prevent cervical cancers by detecting precancerous lesions. These could also detect some cancers early when treatment has more successful. Screening is assisted to reduce mortality for cancers of the cervix and preventing cervical cancer. Most women were diagnosed with women who did not receive yearly cervical cancer screenings. Early diagnosis is extremely important for successful treatments. The current primary screening method for cervical abnormal growth is PAP smear. It is labor-intensive and time-consuming with a significant number of false positives/negatives. In suburban and rural areas of Thailand, it takes 1-3 weeks for patients to get their PAP results [7]. Hence, there is a need for an effective and real-time screening method that gives an early and confident diagnosis.

1.4 Introduction of technologies for cervical cancer detection

The early cervical cancer detection methods that are assisting diagnosis and treatment in a single visit [8]. Visual inspection with acetic acid (VIA) is the most widely available screening use in developing countries. This is a simple test, in which the cervix is examined with the naked eye then application of 3 to 5% acetic acid. After the application of the acetic acid, suspicious areas in the cervix turned white [9][10]. The high-resolution fiber optic microscopes are now available as an alternative to the examination of the cervix which facilitates direct visualization of neoplastic indicators without invasive biopsy. Dyes can provide high optical contrast if applied topically such as proflavine, a fluorescent DNA label. The high-resolution fluorescence imaging of this agent application in tissue could furnish morphologic information such as the nuclear-to-cytoplasmic ratio which is an important parameter used in the histological diagnosis of cancer. There was a lot of history of safe clinical use as a topical antiseptic [11][12], and the agent is composed of acriflavine, which has been used in clinical imaging studies of the cervix.

The high-resolution optical imaging technologies could serve as an appropriate solution for cervical cancer screening [13]. Recently, there was the development of a high-resolution microendoscope (HRME) to eliminate the limitations of conventional methods of cervical cancer screening. The HRME has been evaluated in pilot studies

of oral and esophageal precancer diagnosis by applied proflavine topically to the area and interrogated with a fiber-optic bundle [14][15][16]. The changes in cell morphology could be visualized in real-time on a laptop computer screen.

1.5 The peptide synthesis for cervical cancer detection

Recently, the several techniques of cervical cancer detection and treatment at the molecular level have an important role in the development of diagnostic and therapeutic technologies. It is widely used as a direct in vivo examination and treatment of the patient's body. In vitro laboratory specimen diagnosis, a widely used molecular therapeutics technique, is based on a specific binding principle between the antibody molecule and the target antigen, which is biomarkers of cancer cells. Antibodies are used as molecular probes, labeled with a visual signal carrier, such as a fluorescent dye, enzymes and chromogens for specific diagnosis of cancer cells. Based on research evidence found that the application of p16INK4a [17][18][19][20] as a biological marker of cervical cancer using antibodies as a detection molecule could improve the specificity of the diagnostic techniques and reduce the variance of the interpretation of the sprinkling inspection results each time or for each individual [21][22] Piyawattanametha et al [23], therefore, selected p16INK4a protein as a target molecule to study the development of a specific binding peptide for use in cervical cancer screening. Specifically captured peptides from these research projects can be used for in vivo assays by modifying the labeling of synthetic peptides with a visual signaling agent for endomicroscope detection [24].

1.6 Objective of the project

i. To develop optical fiber bundle-based fluorescence endomicroscopes to be used with the fluorescence-labeled peptides for detecting cervical cancer at an early stage.

CHAPTER 2
REVIEW OF CERVICAL CANCER THEORY

2.1 Cervical Cancer Screening Early

The incidence and mortality of cervical cancer have decreased in the United States for 5 years past. Most of that is because of widespread screening practices. However, 93 to 100 percent of cervix carcinomas compose of DNA from high-risk types of HPV, which have been transmitted by sexual intercourse. Studies of cervical cancer have shown the infection with high-risk HPV types might lead to low-grade or high-grade intraepithelial lesions. High-grade lesions might cause cervical carcinoma if not treated. The purpose of screening is to detect cervical cancers at an early stage, remove high-grade lesions, and prevent potential progression to cervical carcinoma [25].

Nevertheless, in Thailand, the incidence of cervical cancer has not decreased because screening does not cover all vulnerable populations. Quality problems of cellological services diagnosis and treatment after screening is not enough. An important factor that could reduce the incidence and mortality of cervical cancer is to increase screening rates to cover vulnerable populations that have not been tested or tested long ago. In addition to early cancer, pre-cancerous marks are detected, which can be cured.

2.1.1 Method of Cervical Cancer Screening early

The screening method to know of cervical cancer early is to receive yearly regular screening tests. There are 2 popular test methods for cervical cancer screening that are the HPV DNA and Pap smear testing. Regular screening has been prevented cervical cancers and protects women's life from cervical cancer. Early detection exceedingly ameliorates the chances of successful treatment of pre-cancers and cancer stages. Being aware of any signs and symptoms of cervical cancer could assist to avoid late diagnosis.

HPV and Pap tests are performed by doctors to determine the development of a transition to cancer or pre-cancerous stages of cervical cells. These marks can develop into cervical cancer. An HPV test determines whether a woman has an HPV infection,

which can lead to cervical cancer. If the HPV DNA test is positive, this might mean that there is a pre-cancerous change in the cervix. There are several types of HPV tests, called HC2 tests. The Pap test is used to determine if cervical cells are abnormal. Abnormal cervical cells that are verified as low grade to high grade might mean that there is a pre-cancerous stage change in the cervix, which could lead to cervical cancer. One type of Pap test is conventional cytology and the other is liquid-based cytology, depending on the results. If the results are positive, the woman may need a cervical examination or receive surgery to remove pre-cancerous marks. The screening method offers the best chance to get cervical cancer found early for treatment could be successful. Screening could also actually prevent most cervical cancers by finding abnormal cervical cell changes or pre-cancers. Thus, they can be treated before turn into cervical cancer [26].

2.1.2 Age to begin cervical cancer screening.

There are roughly 11 million women in range aged of 20 to 24 years and 25 to 29 years. The overall of cervical cancer among women aged 20 to 24 years is around 0.8% of all new cases diagnosed in this age group compared to among women aged 25 to 29 years which is 4% of all new cases diagnosed. The cervical cancer deaths that cause from a diagnosis at women aged 20 to 24 years is about 0.5% compared with 3% diagnosis among women aged 25 to 29 years.

According to ACS guideline for cervical cancer screening, the ACS recommended that the women begin at age 20 years should receive cervical cancer screening and regardless of the age of first vaginal intercourse. The begin cervical cancer screening has developed over the years with a greater understanding of the disease. However, early cervical cancer screening is important which could be treated before develops into cervical cancer [25].

2.2 Fluorescence microscopy

Since the mid-20th century, the mortality of cervical cancer is declined significantly. Due to the widespread screening practices. Fluorescence microscopy is the analytical instrument that applies the fluorescence spectroscopy technique to visualize fluorescence images at a microscopic level. Fluorescence is a phenomenon

when fluorescent molecules (fluorophore) absorb small wavelengths of light called excitation light and emit small wavelengths of light called emission light. Fluorescence microscopy is accomplished by integrating a powerful excitation light source and fluorescence filters into a microscope.

2.2.1 Principles of Fluorescence

The fluorescence process begins with the absorption of light by fluorescence molecules, followed by the photon emission of fluorescence molecules. The emission energy is comparatively low compared with excitation energy, which proportional to the wavelength of emission and excitation light. Therefore. The excitation light generally longer wavelength than the emission light.

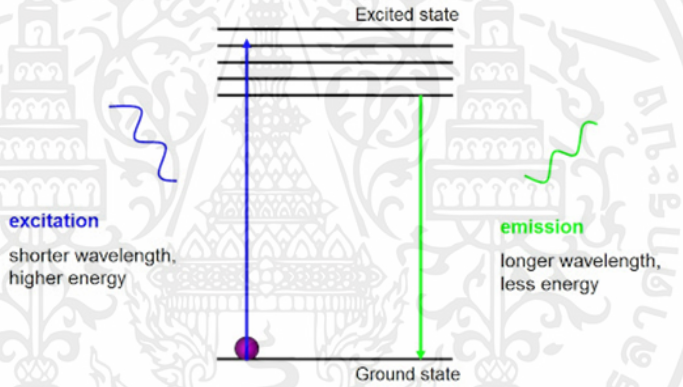

Figure 2.1 Principles of fluorescence [27].

The change of the electron stage from a ground state to an excited state of fluorophores is induced by at least a single photon from an excitation light source. The reverse transition releases a photon of a longer wavelength after relaxation to the lowest energy. Stimulated emission depletion (STED) performs the suppression of fluorescence and transition from an excited state to a higher ground state [27].

2.2.2 Fluorescein

Fluorescein is an organic synthetic substance, characterized by a dark orange or red color which is soluble in water and alcohol. It is commonly used as a fluorescence tracer to indicate locations or traces in biology. The fluorescein can be activated with a wavelength of 494 nm and the longest wavelength at this fluorescein can emitted 521

nm as shown in figure 2.2. There are 3 main types of fluorescein currently used: 1) fluorescein isothiocyanate (FITC) 2) oligonucleotide synthesis 3) 6-FAM phosphoramidite. By fluorescence specific to cancer cells which could be able to identify the specific location of cancer cells as in Figure 2.3 [28].

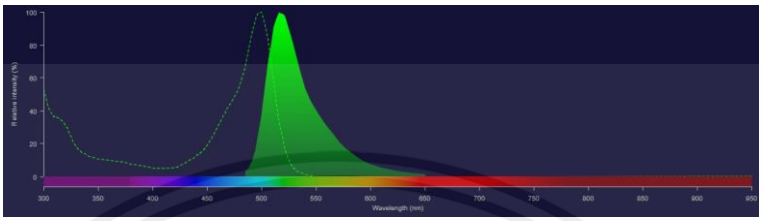

Figure 2.2 Excitation and emission wavelengths of FITC [29].

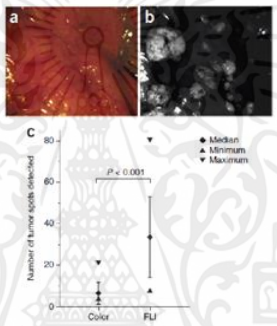

Figure 2.3 Normal and abnormal tumor cells image comparison. (a) Normal color indicates the tumor area (b) Fluorescence image showing only the tumor area (c) Graph showing tumor cell count of each imaging model [30].

A fluorescence microscope is a common instrument to selectively visualize cells for modern cell biologists. It projects a parallel beam of excitation light to the specimen via an objective lens. The beam illuminates the whole specimen with the same intensity to equally excite the fluorophore on the specimen as shown in figure 2.4.

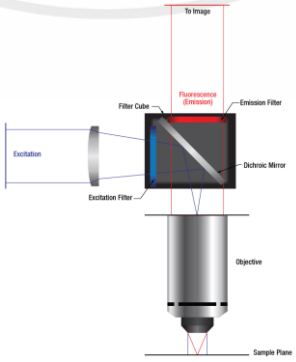

Figure 2.4 Principle of Fluorescence microscopy [27].

In the past, mercury or xenon high-pressure bulbs are used as excitation light sources. In that time requires optical filters to select the specific wavelengths to illuminate the whole specimen. In contrast, newer technologies such as laser scanning microscopes use techniques called point-source illumination. Laser scanning microscopes scan the whole specimen point by point to reconstruct the image from every point. One of the new approaches for excitation light is light-emitting diodes (LEDs)/ The advantages of LEDs are the variety of wavelength control, fast switching, and the long period of a lifetime. The filter wheels can be obviated in an LED-based fluorescence microscope and the confocal microscope depend on the color rendering and the bandwidth of LEDs. The wide-field microscopy operation is image contents are simultaneously viewed or captured by a camera sensor. Due to the simplicity of a wide-field microscope, the low spatial resolution image may be caused by the diffraction limit of optics. Another limitation is wide-field microscope cannot block the camera sensor from out-of-focus light. By the way, a wide-field microscope is still commonly used because of system simplicity and fast imaging. Additionally, the image acquisition rate depends on the photomultiplier system or the camera.

The wide-field imaging requires lower excitation intensity to prevent phototoxicity and photobleaching. It is generally used to visualize specimen in real-time by eyes. But the care must be handled to minimize photobleaching and observation time. The main advantages of a wide-field microscope are affordable price, simplicity, and system flexibility. In contrast, disadvantages of a wide-field microscope are low image resolution, shading artifacts due to illumination. Another problem with a wide-field microscope is the pixel registration of different camera sensor formats [27].

2.3 Optics

2.3.1 Lens

Generally, the light microscope is composed of optical components that function together to magnify the resolution from a macro scale down to a smaller scale, particularly a microscale. It is imperative to understand the general properties of each optical component. The lens is the main optics component to form the image and control the characteristics of the illumination part of the microscope system. The lens that can neglect the thickness of the lens is called a thin lens, which consists of two refracting

surfaces in a single lens element. The principal plane and focal plane of a lens is the plane within the lens and in the focused image, respectively. The simple positive lens that converges the collimated light beam to focus on ray's intersection point is called the focal plane. The distance between the principal plane and the focal plane is called the focal length. In contrast, a negative lens diverges the collimated light to expand the ray, which out-spreads from the virtual focal point.

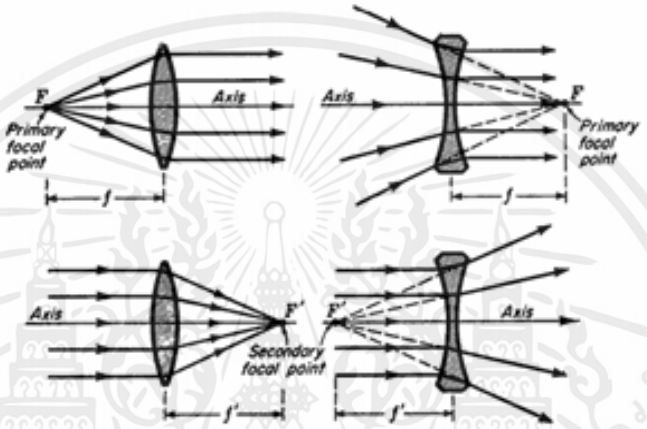

Figure 2.5 Demonstration of focal points for concave and convex lens [31].

The primary focal point is an axial point that the beam coming from when the lens converts the beam to be collimated. In contrast, the secondary focal point is an axial point that collimated the beam passing through the lens and the ray point toward it. Typically, the converging lens and diverging lens have positive and negative focal lengths, respectively. However, for the lens that has the same medium for both sides, the primary and secondary focal lengths are equal. In the case of a single spherical surface, the focal plane is perpendicular to the axis at the focal point [31].

2.3.2 Image forming by thin lens.

Lenses are commonly applied in optical instruments such as cameras, telescopes, and microscopes in order to form images for either capturing or inspecting. The relationship between object and image distance for a refracting surface is determined by

$$\frac{n_1}{p}+\frac{n_2}{q}=\frac{n_2-n_1}{R}. \qquad (2.1)$$

where p is object distance, $q$is image distance which is independent if the angle ray makes with the axis. The results are that all paraxial rays focusing on the same point I.

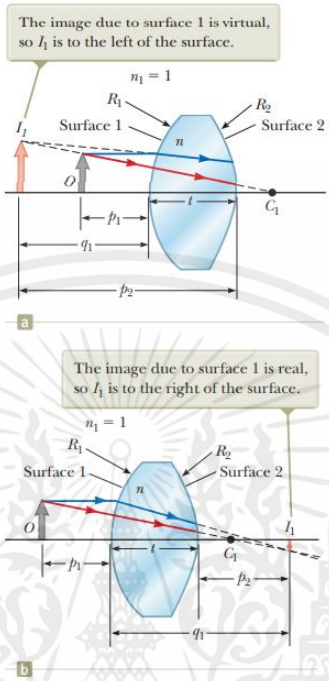

Figure 2.6 Thick lens analyzing. (a) First stage to analyze thick lens. (b) Second stage to analyze thick lens [32].

When light passes through the lens, it is experienced at two surfaces. Consider a lens having refractive index n and two spherical surfaces with radius of R_1 and R_2, respectively. An object is placed at point O at a distance p_1 in front of a first surface. First, analyze the image formation by first surface. Assume that optical system is surrounded by air, then equation 2.2 becomes

$$\frac{1}{p_1} + \frac{n}{q_1} = \frac{n-1}{R_1}. \qquad (2.2)$$

A second surface is analyzed by using equation 2.1, then equation 2.2 becomes

$$\frac{n}{p_2} + \frac{1}{q_2} = \frac{n-1}{R_2}. \qquad (2.3)$$

For a thin lens, the thickness of the lens can be neglected. By this approximation, object distance of second surface is equal to negative of image distance of surface one. Noted that subscripts of image distance and object distance can be neglected to simplify the equation. Then the relationship between these two surfaces is

$$\frac{1}{p}+\frac{1}{q}=(n-1)(\frac{1}{R_1}-\frac{1}{R_2}) \quad (2.4)$$

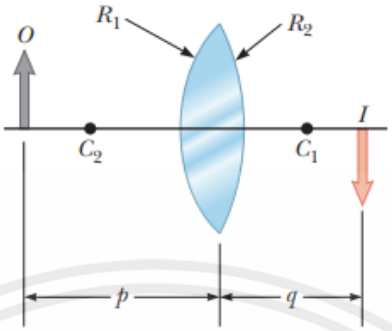

Figure 2.7 Simplified thick lens diagram [32].

The focal length of a thin lens is image distance that corresponds to infinite object distance [32]. Then, let the object distance approach infinity cause image distance approach focal length of the lens. The focal length for a thin lens determined by lens-maker's equation is

$$\frac{1}{f}=(n-1)\left(\frac{1}{R_1}-\frac{1}{R_2}\right). \quad (2.5)$$

The focal length for a thin lens determined by thin lens equation is.

$$\frac{1}{f}=\frac{1}{p}+\frac{1}{q}. \quad (2.6)$$

2.3.3 Image magnification

The geometric construction of the light rays passing through lens cause the magnification of the image is

$$M=\frac{h'}{h}=-\frac{q}{p}. \quad (2.7)$$

where h' is image height, his object height. From this expression, positive and negative magnification is an upright image on the same side of the lens as object and inverted image on the side of the lens opposite the object, respectively [32].

2.3.4 Optical filter

The optical filter is the optics component that allows some optical spectrum to transmit and reject the remaining length spectrum. The filter precision level depends on

the application. The application of optical filters commonly includes microscopy, spectroscopy, chemical analysis, and machine vision. Interference filters have step cut-in and cut-off boundaries. Generally, fluorescence microscopy applies this filter because it has high selectivity. Interference filters are planar sheets of glass coated with multiple dielectric layers. In each thickness layer is half or fourth of the wavelength, which is selectively blocking some specific wavelengths by constructive and destructive interference. Bandpass filters transmit only a selected range of wavelengths that reinforce through constructive interference between transmitted and multiple reflected rays. The remaining wavelengths are bounced back out of the filter. The thickness and refractive index of the optical path of dielectric layers control the selectivity and range of bandpass filters [33].

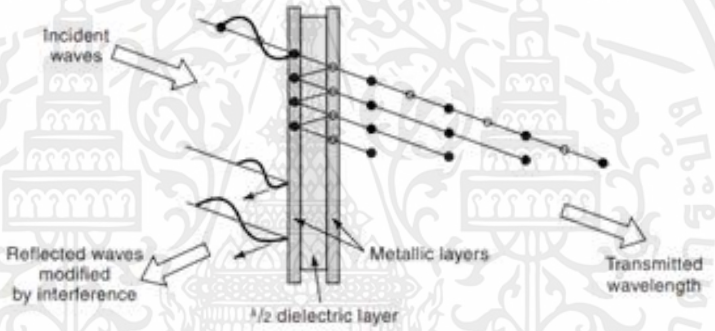

Figure 2.8 Diagram of the thin-film interference coatings filter [33].

2.3.4.1 Optical Density (OD)

Optical density is the term to determine the amount of energy blocked or attenuated by a filter. The value of optical density is inversely proportional to the optical transmission. In fluorescence microscopy, generally use the filter that has optical density more than or equal to 6 [33].

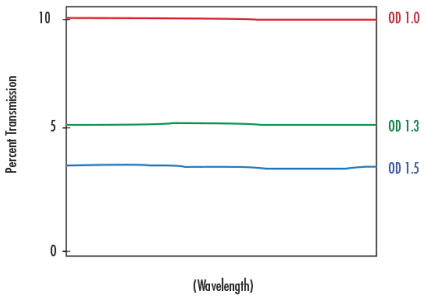

Figure 2.9 Percentage transmission/wavelength of the neutral density filter [33].

2.3.4.2 Central Wavelength (CWL)

Central wavelength is used in defining the bandpass filter by describing the center of transmitted spectral bandwidth [33].

2.3.4.3 Bandwidth

Bandwidth is a range of wavelengths used to denote the spectral band that passes through the filter. Full Width-half maximum (FWHM) refers to the bandwidth, where the upper and lower limit of that bandwidth is more than half of the maximum transmission percentage. The broadband filter that has FHWM more than 50nm is suitable for fluorescence microscopy applications. In contrast, the blocking range is a wavelength interval used to denote the spectral band that is blocked or attenuated by the filter. Optical density (OD) is a term for determining the blocking degree of filters [33].

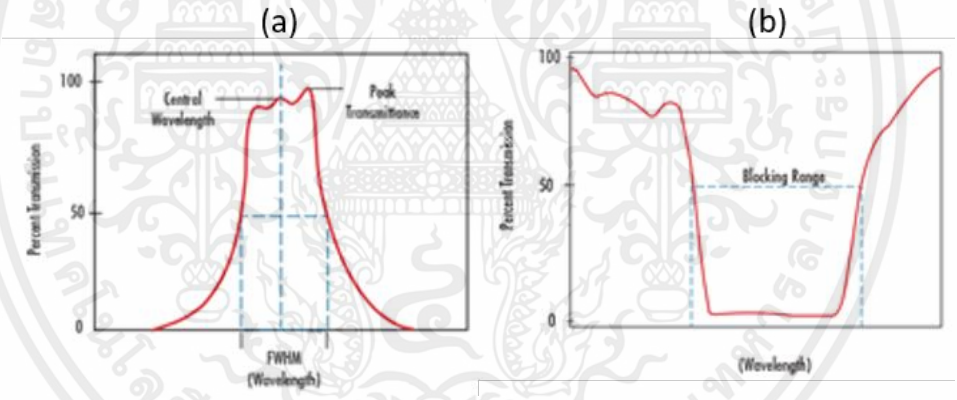

Figure 2.10 Bandwidth of an optical filter. (a) bandpass filter (b) Blocking range of the filter [33].

2.3.4.4 Slope

The slope of the optical filter defines the spectral wavelength in the range where transitions from blocking to transmitting occur in the percentage of the cut-wavelength unit. The slope value depends on the starting point, endpoint, cut-off wavelength [30].

2.3.4.5 Dichroic filter

The dichroic filter is an optical component that can either transmit or reflect the light. The selectivity and the range of both transmission and reflection are depending

on the wavelength. This filter is typically used in short-pass and long-pass applications [33].

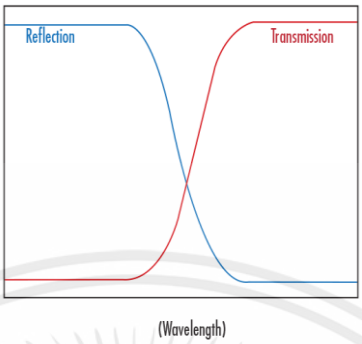

Figure 2.11 Transmission and Reflection / wavelength of dichroic filter [33].

2.3.4.6 Cut-on and Cut-off wavelength

Cut-on wavelength specifies the wavelength where transmission is rising to 50 percent in a long-pass filter. On the other hand, Cut-off wavelength specifies the wavelength where transmission is decaying to 50 percent in a short-pass filter [33].

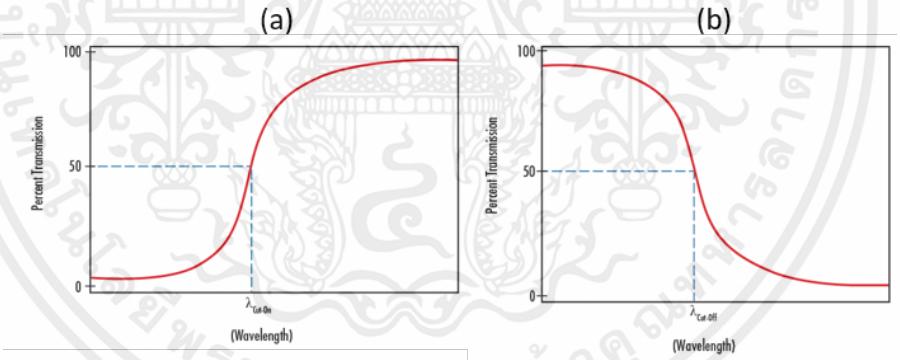

Figure 2.12 Cut-on and cut-off wavelength of an optical filter. (a) Cut-on of long-pass filter. (b) Cut-off of short-pass filter [33].

2.3.5 Optical fiber

Since 1960, optical fibers were first introduced as optical elements. The microscopic structure of the insect eye idealizes scientists that the appropriate fiber bundle can be used as optical waveguides to transfer an image. Charles Kao is the first one who sees the potential of low-loss optical fibers could be a competitor of a metal waveguide and coaxial cable for telecommunication. In 1970, optical fiber lossless becomes suitable for commercial applications by 10 dB/km. The revolutionary concept

from Corning incorporated drove the rapid development of optical fiber communication. Another factor is the material of optical fibers can use very small index changes between core and cladding can guide light more than ten kilometers before reaching the detection limit. Nowadays optical fiber technologies have been applied in both commercial and laboratory application. The demand for optical fibers in engineering and research is exponential growth [34].

2.3.5.1 Principles of operation

Dielectric optical waveguides structures are known as a superset of optical fiber. The optical fiber operation is similar to other waveguides, with the combination of a cylindrical axis of symmetry. The optical fiber can slightly deviate from this symmetry in some specific applications. Figure 2.13a shows the general optical fiber design with lower-index cladding wrapped around a higher-index core. The difference indexes between two layers are required to reflect the light at the interface when the incident angle is greater than the critical angle.

$$\theta_c = sin^{-1}(\frac{n_1}{n_0}) \qquad (2.8)$$

Figure 2.13b shows the geometrical to allow a continuous range of internally reflected rats. The self-interference condition of light must be satisfied to be trapped in the optical waveguide. There are limited light paths that satisfied this condition. The propagating electromagnetic modes of the structure are analogous to these conditions. Geometrical optics can adequately analyze a large number of modes of optical fiber. Maxwell's equations can characterize a small number of modes of optical fiber with the proper boundary conditions for the structure [34].

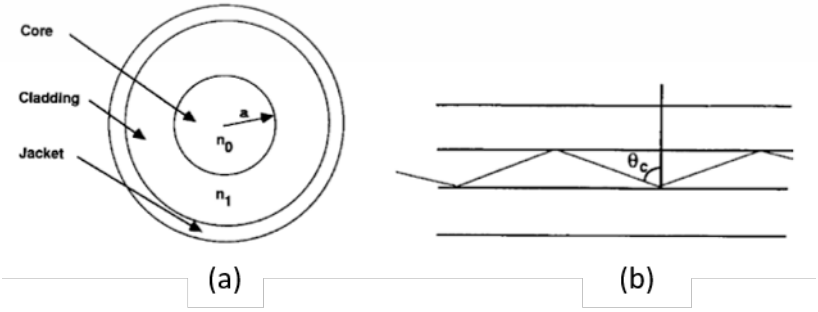

Figure 2.13 Generic optical fiber design and operation [34].

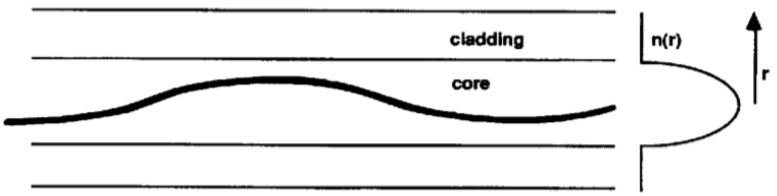

Figure 2.14 Ray path in a gradient- index fiber [34].

2.4 Modified secant method

Modified secant method is one of the open root finding techniques in numerical methods. It is based on the Newton-Raphson method, which has the evaluation of derivatives. Main disadvantage of Newton-Raphson method is sometimes it is difficult or inconvenient to evaluate due to the complication of derivatives. Modified secant methods applied the concept of Newton-Raphson method, but approximate the derivative by fractional perturbation of the independent variable instead of using real derivative. The Newton-Raphson method equation and fractional perturbation of the independent variable equations are shown in equation 2.9 and equation 2.10, respectively.

$$x_{i+1} = x_i - \frac{f(x_i)}{f'(x_i)} \quad (2.9)$$

$$f'(x_i) \simeq \frac{f(x_i + \Delta x) - f(x_i)}{\Delta x} \quad (2.10)$$

Then substituted derivative approximation (equation 2.10) to Newton-Raphson method (equation 2.9) to form Modified secant methods (equation 2.11).

$$x_{i+1} = x_i - \frac{f(x_i)\Delta x}{f(x_i + x) - f(x_i)} \quad (2.11)$$

Numerical errors arise from the use of approximations to represent exact mathematical operations and quantities which is the discrepancy between the truth and the approximation as in equation 2.12.

$$E_t = true\ value\ -\ approximation \quad (2.12)$$

E_t is the exact value of the error, but in some applications significant magnitudes of the quantities are different. Then normalize the error to the true value is introduced as true fractional relative error which is described in equation 2.12.

$$\varepsilon_t = \frac{E_t}{true\ value} \quad (2.13)$$

Since, modified secant method is the method for searching the root of the function. It must determine the stop criteria of the solution. The stopping criteria is the threshold value of the error that generated solution must be lower. One issue in the stop criteria is that the error for validating the error must always be positive. So, the error must be absolute before compared with the stop criteria [35].

2.5 Image processing

Image processing is a transformation applied to an input image and output image is returned to perform an operation on an image and enhance an image. Image processing focuses on two major tasks. First is the improvement of image data information for human interpretation and second is the processing of image data for storage, transmission, and representation [36].

2.5.1 Contour

Image contouring is the process of identifying the structure of objects in an image which could help us identify the shape of the object [37].

2.5.1.1 Definition and properties of the contour

Outline presenting or bounding the shape or form of an object in an image called contour. Practical tasks such as object recognition can be solved by contour detection algorithms in some conditions. Nowadays, numerous researchers have worked on problems, then gained significant achievements. The contour detection result is the boundary object's curve from a binary image. A contour in the image is a boundary where pixels change from one object to another.

Furthermore, edges inside an image are detected by changing the value of the image function such as brightness or color. In other words, edge detection algorithms are the low-level technique to achieve the boundary or contour image. Figure 2.16 shows the four classical means by which contours are observed as luminance change, texture change, perceptual grouping, and illusory contour, respectively. In luminance

change and texture change, contours are detected by region boundaries. On the other hand, perceptual grouping and illusory contours are detected by global relations [38].

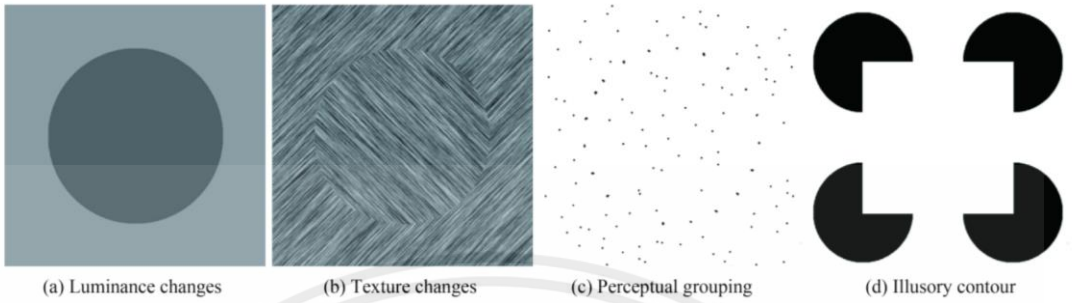

Figure 2.15 Four classical means of observing contours [38].

2.5.2 Delaunay triangulation

Triangulation is a method to divide the surface of an image into regions that shared common characteristics between each other. Characteristic types depend on the triangulation type. The divided surfaces from Delaunay triangulation are suitable for image processing applications. Triangulation divides the surface into pieces of a triangle that share edges with neighbor triangles as shown in figure 2.17 and figure 2.18.

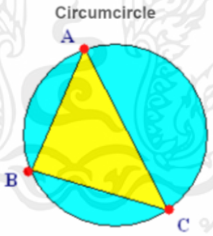

Figure 2.16 The circumcircle of a triangle is the circle that passes through all of the triangle's vertices (A, B, C) [39].

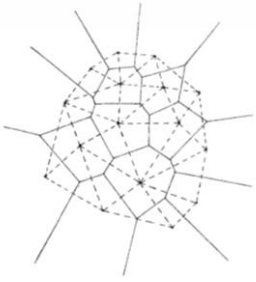

Figure 2.17 Delaunay triangulation (dashed lines) [40].

Delaunay triangulation strength against other types is the maximization of the minimum angles of triangles on the surface. In this way, the triangles have equiangularity, which prevents cases that some triangles that are long and thin. So, triangles of the surface from Delaunay triangulation are geometrically balanced [39][40].

2.5.3 Clough-Tocher interpolation

The Clough-Toucher interpolation technique is based on the finite element method of numerical analysis. The Clough-Tocher method is a standard technique for constructing a sectionally polynomial surface which interpolates the position and function above a triangulation of the plane to obtain a consistent mixed partial derivative at the vertices of the triangulation. The points are first triangulated to form a network of triangles. A bivariate polynomial is defined over each triangle and creates a surface made up of a series of triangular Clough-Tocher surface patches.

Since the Clough-Tocher scheme is a local scheme, it has the advantage of speed. Even very large sets of points can be interpolated quickly. It also tends to give a smooth interpolating surface which brings out local trends in the dataset quite accurately [41].

CHAPTER 3
METHODOLOGY

3.1 Planning and scope

2 Semester	Month							
Plans/activities	1	2	3	4	5	6	7	8
1. Literature review of fiber bundle optical endomicroscope illumination, detection, and CMOS systems.	x							
2. Optical Alignment of fluorescence endomicroscope system.		x	x					
3. Fiber-optic bundle polishing and cleaving.				x	x			
4. Graphical user interface development				x	x	x		
5. Test fluorescence endomicroscope without fluorescence dye and improve the system.						x		
6. Optimized fluorescence endomicroscope systems to be used with fluorescence dye.							x	
7. Test software functionality							x	x
8. Test fluorescence endomicroscope with fluorescence dye.								x

Table 3.1 Planning and scope.

3.2 Design Methodology

This project is an experimental based project that has conceptual framework in Figure 3.1. We will start with the development of the endomicroscope part which will be based on the Fiber Optical Endoscope (FOE) and conceptual designs are explained below.

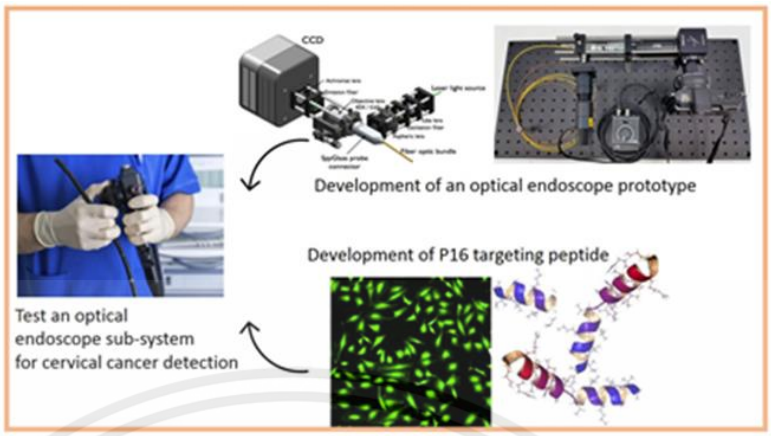

Figure 3.1 Conceptual framework of the project.

3.3 Fiber Optic Fluorescence Endomicroscope

Currently, optical fiber applications are increasing especially within medical devices. Fiber Optic Fluorescence Endomicroscope is an example of an imaging method that uses either a single-mode optical fiber, micro-optics, and a light source as a medical imaging instrument for disease diagnosis. In general, a single-mode Fiber Optic Fluorescence Endomicroscope provides high-resolution images with a complex design of micro-optics and limited field of view (FOV). On the other hand, the Fiber Optic Fluorescence Endomicroscope applied a fiber bundle provides moderate-resolution images with simple micro-optics design and larger field of view (FOV).

As a result, the majority of Fiber Optic Fluorescence Endomicroscope is limited by optical fiber type. Furthermore, adding multi-wavelength light sources and special design micro-optics could be useful for imaging of fluorescence Fiber Optic Fluorescence Endomicroscope. This multi-wavelength emission is obtained from fluorescence compounds used for target-specific cancer types react to specific

wavelengths as a study of uterine cervix biopsies was imaged with a multispectral fiber bundle endomicroscopy.

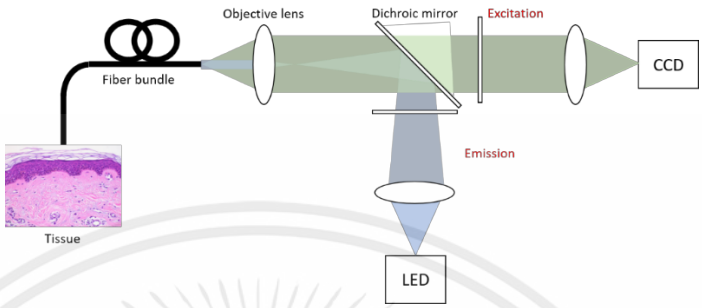

Figure 3.2 The schematic of fiber optic fluorescence endomicroscope system.

A schematic diagram of fiber optic fluorescence endomicroscope system is shown in figure 3.2. This is generally based on Fiber-Optic Fluorescence Microscope [42]. The excitation light source (Thorlabs, M490L4) has nominal wavelength at 490 nm, output power of 240 mW when driven at 350 mW, FWHM of 26 nm. The light source is powered by power supply (Thorlabs, LEDD1B) with a max drive current of 1200 mA. The excitation light is filled back aperture of the objective lens by an aspheric condenser lens (Thorlabs, ACL2520U) which has focal length of 20.1 mm and NA of 0.60. The collimated image from the objective lens (Olympus, MPLN20x) is focused by an AR coated achromatic doublet lens (Thorlabs, AC254-150-A) which has a focal length of 150 mm. This lens's Anti-Reflection (AR) coating range is between 400 and 700 nm. This coating reduces reflectance of the light within wavelength range mentioned previously, this helps to decrease glare and increase the sharpness and image contrast [43]. The image is focused on a monochrome CMOS camera (FLIR, GRASSHOPPER®3). The position of AR coated achromatic doublet lens and the position of aspheric condenser lens should be placed at its focal length away from CMOS camera and excitation light source, respectively. The position of the fiber bundle (Fujikura, FIGH-10-350S) terminator should be placed at working distance of objective lens which has magnification of 20X, numerical aperture of 0.4, working distance at 1.3 mm, and transmittance/wavelength graph as shown in figure 3.3.

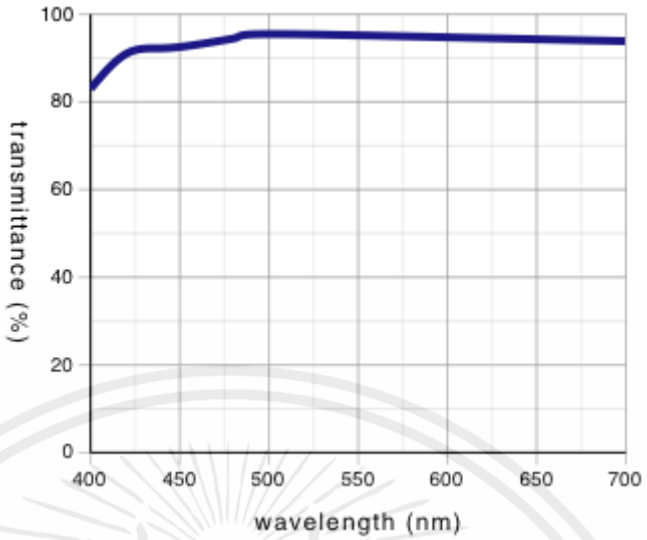

Figure 3.3 The graph of transmittance/wavelength of objective lens (Olympus, MPLN20x) [44].

The filters set for the fiber optical fluorescence endomicroscope system must be matched with fluorescein isothiocyanate isomer I (Sigma Aldrich, F7250). The maximum excitation and emission wavelength is 492 and 518 nm, respectively [45]. The absorbance/wavelength graph is shown in figure 3.4, the secondary vertical axis is a reference excitation and emission band of Fluorescein isothiocyanate (FITC) [46]. In order to perform FITC fluorescein inspection, the fiber optical endoscope system must have appropriate light source and fluorescence filter set. The excitation filter (Thorlabs, MF497-16) is a bandpass filter with center wavelength is 497 nm and FWHM is 16 nm, which covers the peak excitation region of FITC fluorescein as shown is figure 3.4. The emission filter (Thorlabs, MF530-43) is a bandpass filter with center wavelength is 530 nm and FWHM is 43 nm, which covers the peak emission region of FITC fluorescein as shown is figure 3.4. The dichroic filter (Thorlabs, MD515) serves function to integrate optical pathway of emission and excitation part of reflectance mode of fluorescence microendoscope. This dichroic mirror has a reflection band between 470 and 490 nm and transmission band between 525 and 700 nm. Even though these filters have some non-calibrated wavelength region, when they function together, they support each other to perform FITC fluorescence microscopy. The transmittance/wavelength graph of these filters is shown in figure 3.4. The primary vertical axis is the reference

for the transmittance percentage of filters. Figure 3.4 The graph of transmittance/wavelength of objective lens.

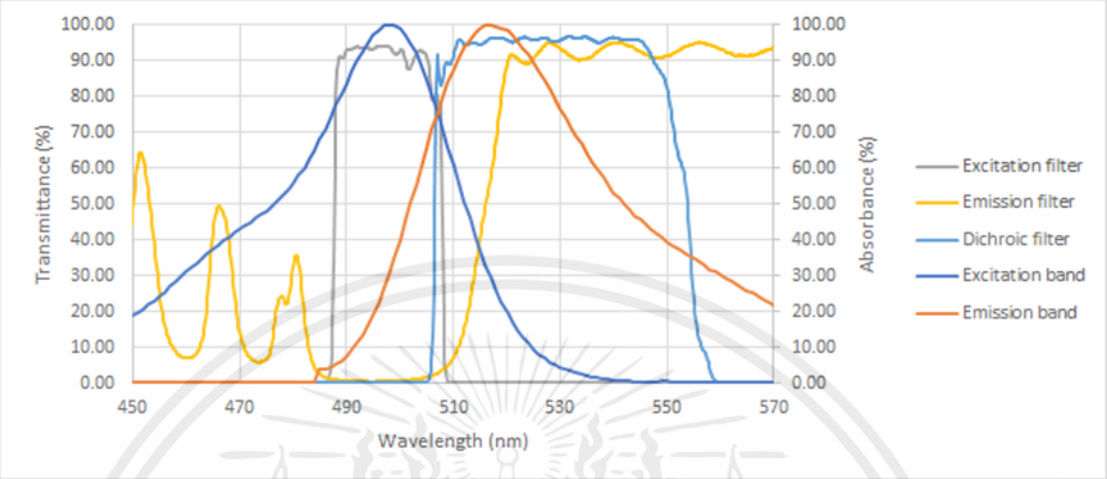

Figure 3.4 The graph represents transmittance and absorbance against wavelength of fluorescence microscopy and FITC.

In practical terms, it is very hard to place the lens at the actual focal point because the tolerance in mechanical parts and the principal plane of the lens is not determined by the lens manufacturer. The alternative way to determine the approximation of the lens position is to use simple focal length approximation. According to the reference [47], they do not provide the object length to be focused on in step 4. The problem of this approximation is the error of this method is not determined. This error can lead to a coating shift of thin film coating filters because interference coatings are sensitive to angle of incidence. When the incidence angle increases, the spectral characteristic is shifted to a shorter wavelength [48]. Also, filters manufacturers recommended working in the collimated ray condition to perform the desired efficiency and accuracy of filters [49]. So, to determine the error from infinite plane approximation in practice is necessary. By error calculation, it can apply the concept of numerical method to find appropriate length of the image for positioning the tube lens with acceptable error. In this project, a modified secant method is used to determine the minimum object distance required to focus on for tube lens positioning with acceptable error. To apply a modified secant method to the thin lens equation. The first thing is to determine the function $f(x)$of this method by using a thin lens equation. In order to use thin lens equation, it must be in terms of $q(p)$. Then the thin lens equation becomes equation 3.1.

$$q(p) = 1/(\frac{1}{f} + \frac{1}{p}) \quad (3.1)$$

After rearranging the equation, the next thing to do is adjust the offset of the equation with appropriate value. Since, the focal length of the tube lens is 150 mm, the identical value for both focal length and image distance is 150 mm, when these two parameters are this value object distance becomes infinity. To be applied with a root finding method, equation 3.1 must be subtracted by its own focal length. Then the thin lens equation for modified secant method is written in equation 3.2.

$$q(p) = \frac{1}{\left(\frac{1}{f} + \frac{1}{p}\right)} - f \quad (3.2)$$

The way to calculate the error for this method uses true fractional relative error. The true value for image distance is focal length. The value from modified secant method is substituted back to equation 3.1 to calculate the image distance as approximate value.

3.3.1 Fiber Optic Cable Assembly, Cleaving, and Polishing

Begin to cut the furcation tube approximately 26 mm. Strip the end of the furcation tube using a stripping tool, exposing Kevlar threads and inner tube as shown in figure 3.5a. Trim the inner tube as same as the length of the outer tube as shown in figure 3.5b.

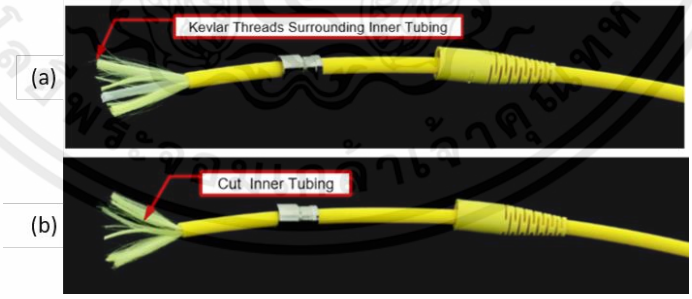

Figure 3.5 The furcation tubing. (a) The furcation tubing after stripping 13 mm of the outer tube. (b) The inner tube is trimmed close to the length of the outer furcation tube [50].

Next step, gently push the optical fiber through the inner tube and make sure that the optical fiber does not get caught inside the furcation tube. Be cautious not to push too quickly or too hard that may cause optical fiber break. Inject the epoxy into the back of the connector until overflow out of the ferrule hole as shown in figure 3.6.

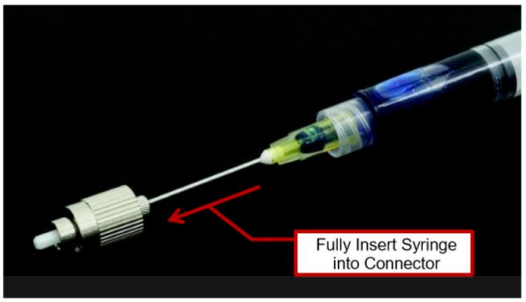

Figure 3.6 Injecting epoxy into the connector [50].

Slide the fiber out of the furcation tube about 50 mm. Be careful to push the connector onto the fiber while slowly rotating the connector. After that crimp sleeve over the back end of the connector and the Kevlar threads together then secure the crimp sleeve as shown in figure 3.7.

Figure 3.7 Secure the crimp sleeve [50].

Next, scoring the optical fiber by holding the connector and using a fiber scribe to score as shown in figure 3.8. Lightly score the fiber above the epoxy bead and gently squeeze the fiber tip then pull along the axis of optical fiber. After scoring the optical fiber, the cleaving method should be easy.

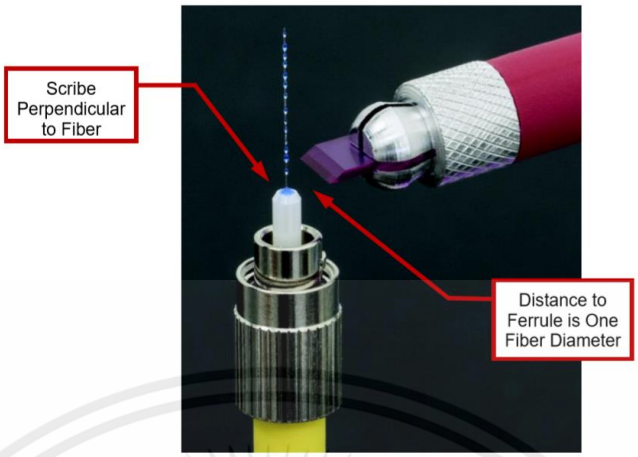

Figure 3.8 Scoring the optical fiber [50].

After optical fiber assembly finished, then continue to polish optical fiber by placing a sheet of the polishing film on the glass plate then polish from roughly polishing film to smoothing polishing films. Polished until the epoxy bead is removed from the ferrule tip. After finished polishing in each level of polishing film, this should be clean the polishing plate and disc with isopropyl alcohol. Place three to four drops of distilled water on one side of a new polishing film. Apply light pressure on the connector, then polishing the optical fiber in a traversing figure eight pattern, moving towards the dry end of the film as shown in figure 3.9. When finished polishing, remove the connector from the polishing disc and clean the connector ferrule with isopropyl alcohol. Testing the optical fiber by microscope inspection [50].

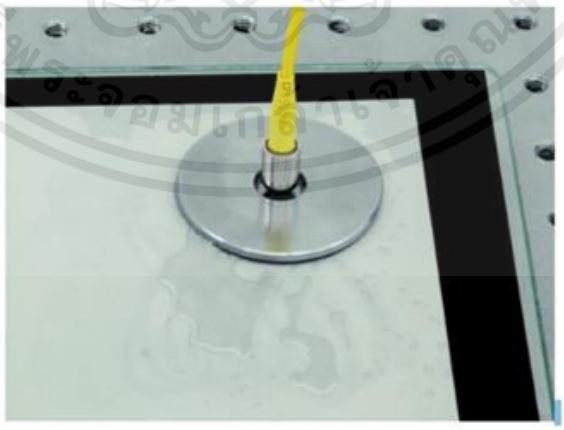

Figure 3.9 Optical fiber polishing [50].

3.4 Preparation of fluorophore and FITC labeled microsphere.

Currently, the types of cancer screening techniques at the molecular level are an important role in the development of diagnostic and therapeutic technologies. There was widely used both directly in vivo and diagnose the test from the patient in the laboratory. Current molecular surveillance techniques rely on the principle of the specific bind between antibody molecules and target antigens, which are biomarkers of cancerous tissue. Antibodies are used as molecular probes labeled with visual signals such as fluorescent, enzyme, and chromogen to use a specific diagnosis of cancerous tissue [51].

According to research [52], proflavine use as a solution that is topically applied to the cervix for colposcopic examination. The concentration of proflavine is 0.01% w/v in sterile phosphate-buffered saline. Proflavine could absorb at 445 nm. The filter set of our fiber optical endomicroscope system must be matched to the solution that was applied to our work, which describes in section 3.3. Our experiment using FITC (fluorophore) and fluorescein isothiocyanate isomer I (FITC labeled microsphere) stained on the sample which used the same concentration as proflavine for testing our fluorescence endomicroscope. The contrast agent was applied to the sample to be imaged.

3.5 Software methodology

The software methodology section describes image processing algorithms and the graphical user interface (GUI) implementation. The medical personnel operate the camera via GUI. The application tasks are streaming camera image, real-time processing, capturing the image, and systematically saving the image. The inter-core spacing of the fiber bundle causes fiber-pixelation artifacts as a honeycomb pattern. The image processing technique is one approach for reducing the honeycomb pattern of the fiber bundle.

The desktop application uses Python 3.8 [53] as the framework for implementation. The external library requirement for the desktop application includes PySpin, EasyPySpin, PyQt5, NumPy [54], OpenCV, and SciPy. PySpin is the Spinnaker software development kit to control the FLIR camera. EasyPySpin is the library for wrapping PySpin camera classes to assimilate to the OpenCV camera classes. PyQt5 is the library for GUI development on the python framework compatible

with the Qt application framework. The remaining external libraries provide calculation and computer vision commands. Furthermore, the internal libraries handled the remaining tasks.

Multithreading is necessary to prevent the freezing GUI from real-time image processing. The background thread is intended to receive and modify images from the camera, then forward either raw images or processed images to display on GUI. The main thread functions as an interactive tool to communicate between medical personnel and the camera.

3.5.1 Image processing

Image processing algorithms serve the function to eliminate the inter-core spacing of the fiber bundle. The inter-core spacing of the fiber bundle interrupts the continuity between pixels of the image from the fiber bundle. Two algorithms are applied to the software for filling the inter-core spacing of the fiber bundle.

The first image algorithm is based on morphological image processing, where the inter-core spacing is filled by applying the dilation method. The dilation method finds local maxima by convolution of the image by the given kernel, subsequently filling pixels of the image inside the kernel by each local minimum [55]. The figure 3.10b shows the flowchart to apply the image dilation method to real-time processing. The dilation image processing is directly applied to the raw image, subsequently emitting dilated image signals.

The second image algorithm is based on the two-dimensional interpolation method, where the inter-core spacing is filled by values obtained from interpolation pixels of fiber optics cores. The figure 3.10c shows the flowchart to apply the image interpolation method to real-time processing. The localization of fiber optics cores of the fiber bundle is required to access the intensity values of every fiber optics core. The fiber bundle structure image is used as a reference image to localize every fiber optics core. Coordinates of fiber optics cores can be identified by finding contours of the fiber bundle structure image, then finding the circles from contours data [55]. The result is the coordinates list of every fiber optics core inside the fiber bundle. The coordinates list is used to access the intensity values of any fiber bundle image. Until this stage, every parameter required to interpolate is resolved. The final step is to reconstruct the

image from the intensity and coordinate of fiber optics cores by the two-dimensional interpolation method [56], then emitting interpolated image signals.

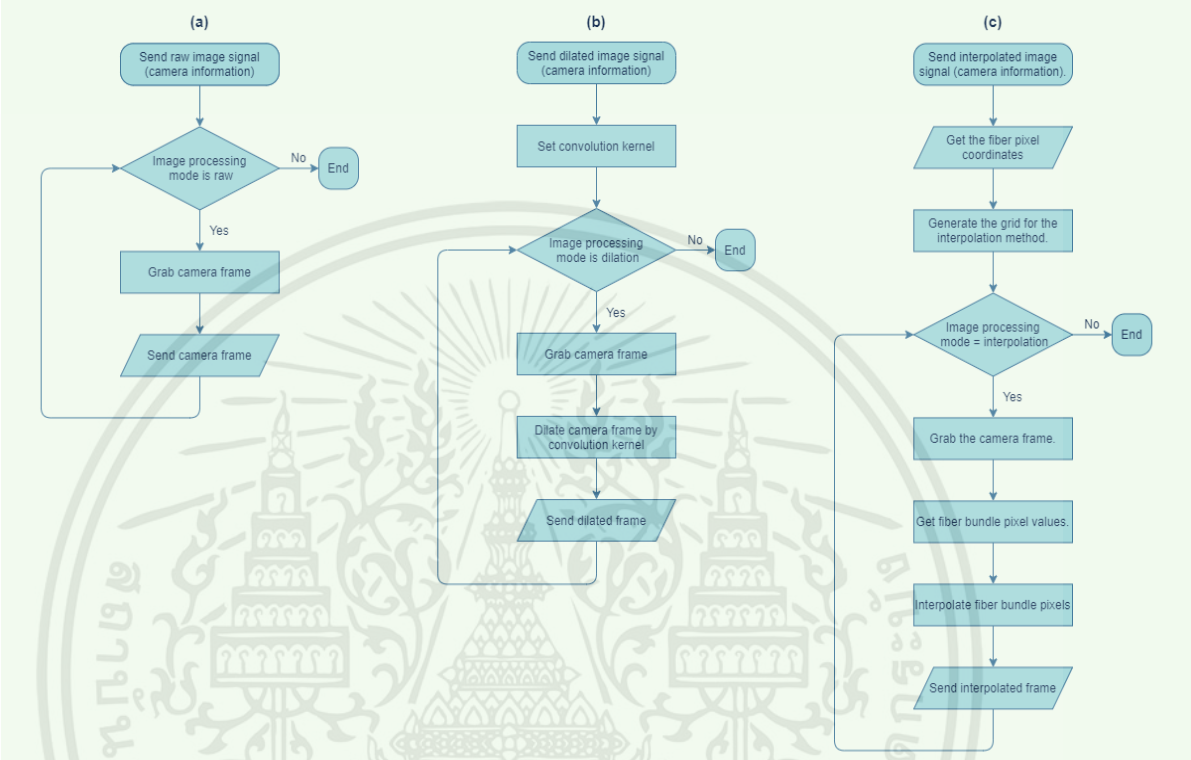

Figure 3.10 Flowcharts of real-time imaging and image processing algorithms.

3.5.2 Graphical User Interface (GUI)

GUI provides the functions to assist a user for show, capture and systematically store on local storage. Separate folder to store images of each case is necessary to organize images to be in the desired directory. The login window is used to collect the patient ID, case ID, patient name, and patient surname to generate a folder based on those parameters. The directory will be created after the login button has been clicked. The created directory is named as the string of patient ID joined with patient name and patient surname. Furthermore, it contains a subdirectory named as case ID. The flowchart of the login window shown in the figure 3.11a. Another window of GUI is the camera window. It functions as the window to view and control the camera. It consists of camera frame, image processing mode selection, and capture button. The camera frame receives and displays images from background thread. The image processing mode selects one background thread from three of it to be running. Each

background thread function is to stream either raw image or dilated image or interpolated image to the main thread. Background threads algorithms and flowchart are described in section 3.5.1. The last function of the camera thread is to capture the image from the camera. Three images are stored when capture button is pressed. Those images are raw image, dilated image, and interpolated image of current camera image. The criteria to generate the image names to avoid image replacing is use current date, current time and image processing mode joining together as image name. The flowchart of the camera window shown in the figure 3.11b. The flowcharts in figure 3.11c describes login window, and camera window function together.

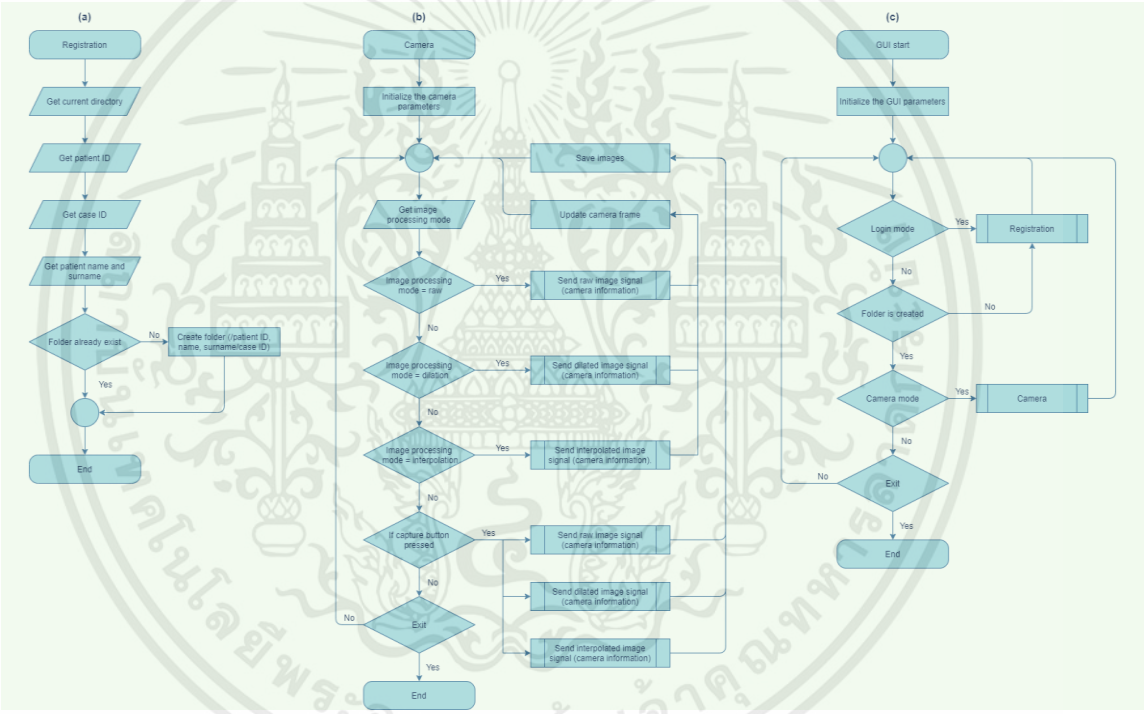

Figure 3.11 Flowcharts of GUI

CHAPTER 4
EXPERIMENTAL RESULT

This chapter describes the development and implementation of fluorescence endomicroscope systems-based fiber-bundle, a system that enables high resolution cellular imaging of cervical cancer cells stained with fluorophore which we have used an image processing method to increase efficiency and enhance the image results. In this chapter, we present a testing method and its results that show the biological image and show the calculation method. Furthermore, this chapter shows graphical user interface development and image processing that we applied to our research.

4.1 Schematic and real setup

The system has described in section 3.3. Our system is a fiber optic fluorescence endomicroscope that can acquire images of tissue in cellular resolution. As shown in figure 4.1, the FOE consists of a flexible 350 um diameter fiber bundle of Fujikura FIGH-10-350S coupled to a light source and a digital CCD camera. The centered 490 nm LED provides excitation light to illuminate fluorescence molecules; fluorescence emission from fluorescence molecules is transmitted from the tissue to the FOE system via fiber bundle, transmitted through a dichroic mirror, and focused onto an optical sensor of the CCD camera by an objective lens and a 150 mm tube lens. Images are transferred to a laptop. When assembled correctly, the system will appear as shown in figure 4.2.

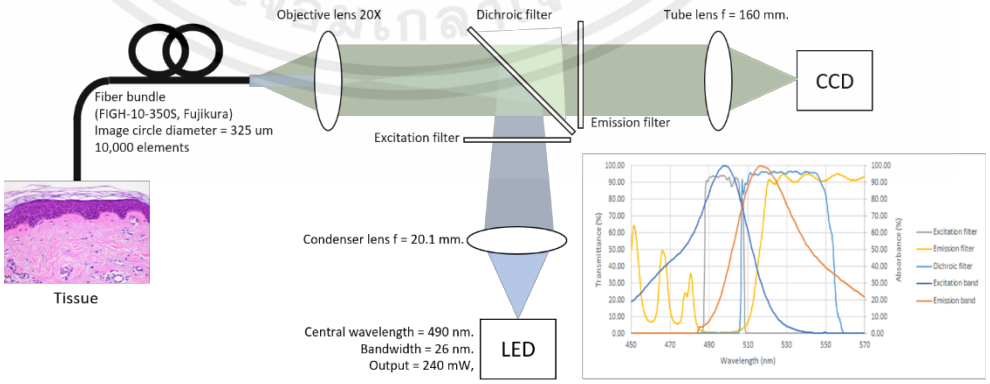

Figure 4.1 The schematic of fiber optic fluorescence endomicroscope system.

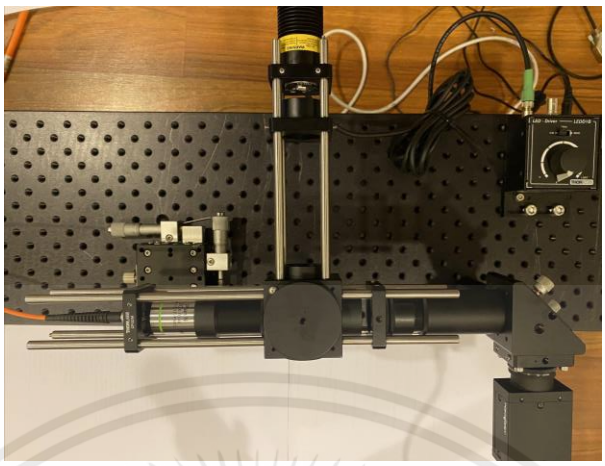

Figure 4.2 A demonstrates of fiber optic fluorescence endomicroscope system.

4.2 Calibration results

4.2.1 CCD camera and tube lens calibration

Tube lens position is defined by the length between the CCD camera and tube lens that focuses the image from an infinite plane as shown in figure 4.3a. In order to get precise tube lens position, the object distance should be far away from the tube lens. Then we decided to use a modified secant method to compute the minimum requirement of object distance required to get precise tube lens position. The stopping criteria is 1% true fractional relative error. The result is the object distance must be at least 15.88m. in order to get image distance within 150±1%mm as shown in figure 4.3b.

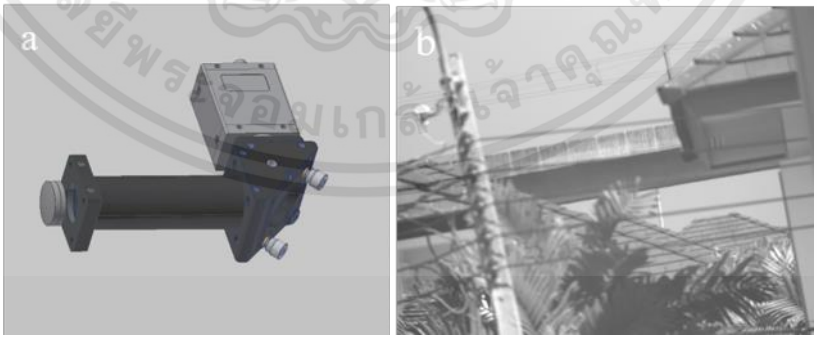

Figure 4.3 Infinity plane calibration result. (a) 3D schematic of CCD camera and tube lens calibration. (b) Calibration image of CCD camera and tube lens.

4.2.2 Light source calibration

In figure 4.4 show a 3D schematic of light source calibration. Illumination methods in optical microscopy are critical illumination and Köhler illumination. The

problem of critical illumination is the image of the light source appearing on the objective lens focal plane because the light from the light source is focused by an objective lens, then the beam is non-uniform as shown in figure 4.5b. In contrast, Köhler illumination provides a uniform beam profile because the light after the condenser lens is collimated by an objective lens as shown in figure 4.6b.

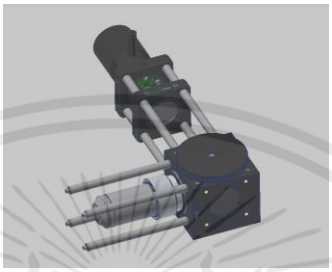

Figure 4.4 3D schematic of light source calibration.

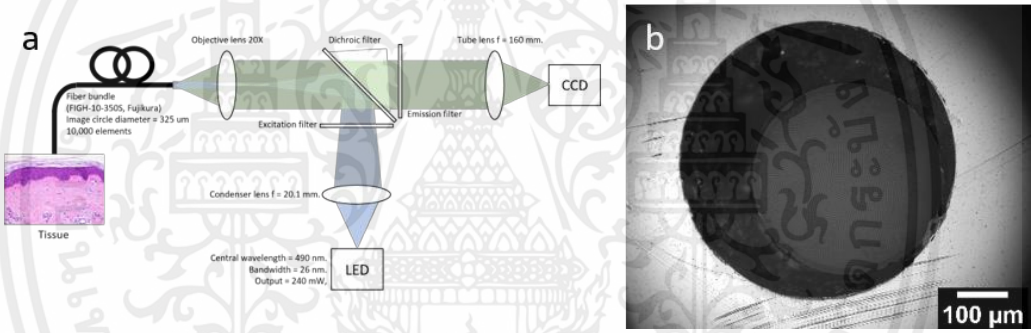

Figure 4.5 Critical illumination result. (a) Diagram of critical illumination (b) Critical illumination result at focal plane of objective lens.

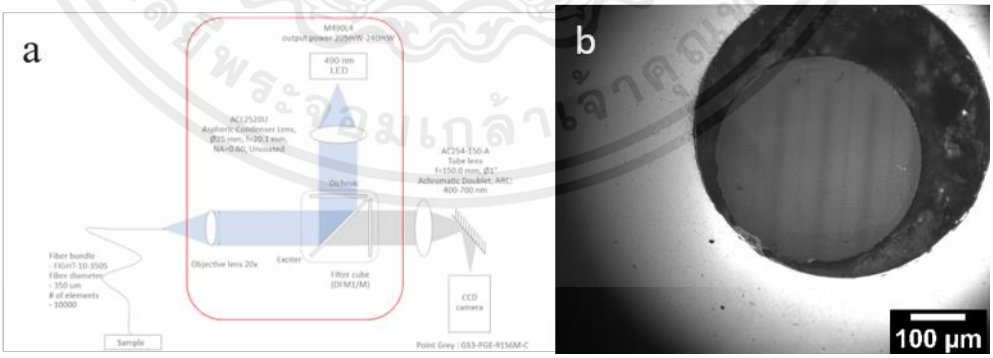

Figure 4.6 Köhler illumination result. (a) Diagram of Köhler illumination (b) Köhler illumination results at the focal plane of the objective lens.

4.3 Fiber bundle polishing and cleaving.

The purpose of fiber optic polishing, and cleaving is to get good fiber optic termination. Thus, the polishing and cleaving are extremely important to fiber optic.

4.3.1 Fiber polishing at proximal end

Fiber polishing is the most critical step in the termination process to get the connector end face flat and clean which has a direct impact on optical performance. The polished the fiber bundle done by following the instruction of Thorlabs and the result shown in figure 4.7.

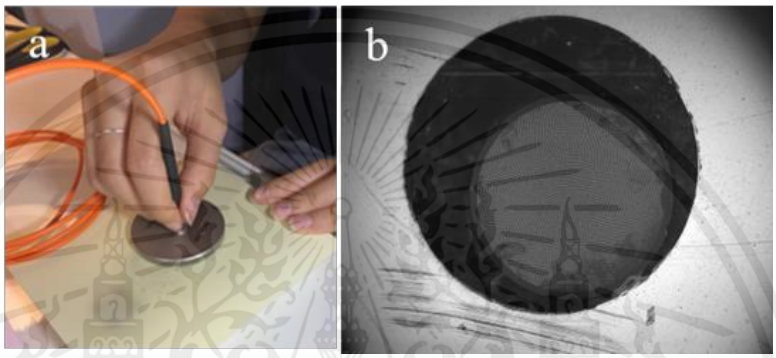

Figure 4.7 Fiber polishing method and result. (a) Fiber-optic bundle polishing method (b) Result of fiber-optic bundle after polishing

4.3.2 Fiber cleaving at distal end

Fiber optic cleaving is a cutting of fiber optic termination process which cut by scoring on the fiber optic surface and cleave with perpendicular to fiber optic. In figure 4.8 showing the distal end of the fiber-optic bundle after cleaving.

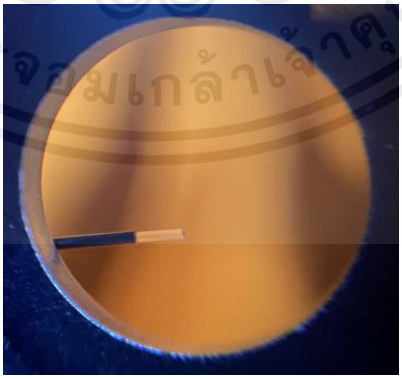

Figure 4.8 The distal end of the fiber bundle

4.4 Fiber bundle checking

Fiber bundle checking showed the flatness of the surface of both proximal end and distal end of fiber bundle. Distal end and proximal of fiber bundle inspected by using Phonescope and Fiber Inspection Scope (Thorlabs, FS201). Coaxial illumination mode of fiber inspection scope results as shown in figure 4.9a shows the high-detail inspection for polish details and smaller scratches. Oblique illumination mode of fiber inspection scope results in figure 4.9b shows cleanliness and core condition of ferrule.

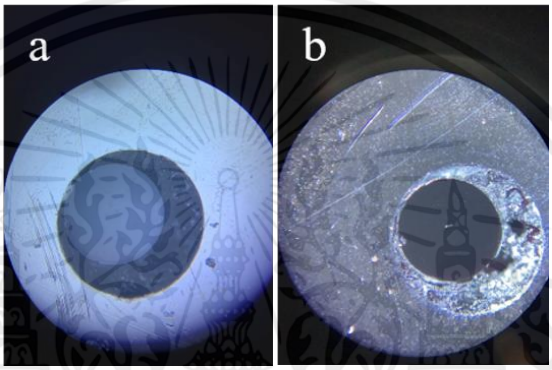

Figure 4.9 Proximal end of the fiber bundle. (a) Coaxial illuminated image of fiber-optic bundle proximal end. (b) Oblique illuminated image of fiber-optic bundle proximal end.

4.5 Fiber optic fluorescence endomicroscope system testing

4.5.1 Endomicroscope resolution measurement

The resolution of the endomicroscope is measured by using a resolution test target (Thorlabs, R1DS1N). This resolution test target is not fluorescence labeled, then additional illumination is required in order to inspect the resolution test target. The resolution test target is placed at the focal plane of fiber-optic bundle distal end. Additional Cyan LED (Thorlabs, M505L4) is used to emulate the emission light of FITC. Cyan LED has nominal wavelength and FWHM of 505 nm and 37 nm, respectively. The Cyan LED is placed after the resolution test target. The real setup shown in figure 4.10. Qualitatively measurement of endomicroscope resolution is 128.0 lp/mm (3.91 um) as shown in figure 4.11.

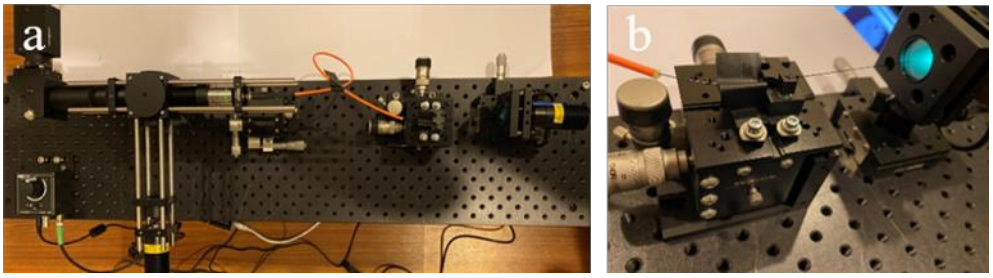

Figure 4.10 The real set up

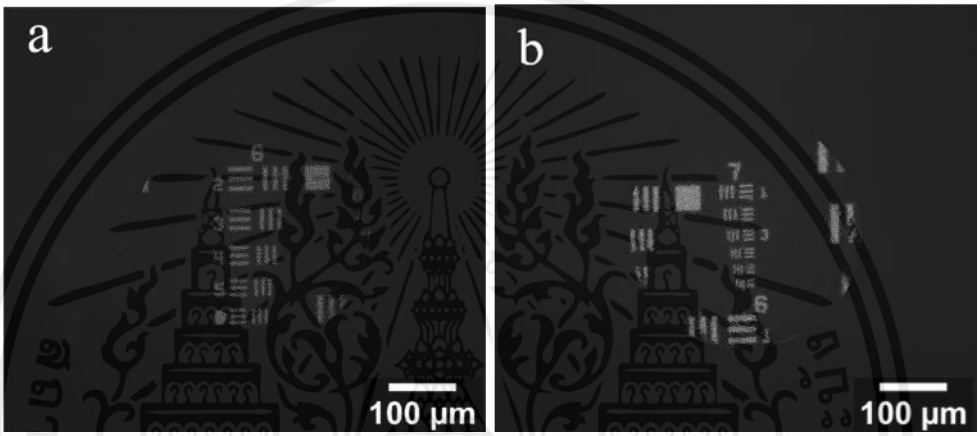

Figure 4.11 Resolution test target results. (a) Group 6 image of negative resolution test target. (b) Group 7 image of negative resolution test target.

4.5.2 Fiber optic fluorescence endomicroscope system testing with FITC labeled microsphere(beads) and fluorophore (FITC).

FITC labeled microsphere of 1% concentration and 10% concentration prepared by dilute it with distilled water as shown in figure 4.12.

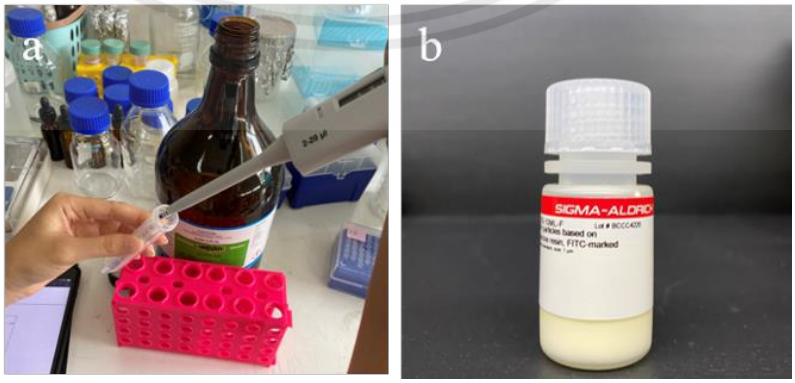

Figure 4.12 FITC labeled microsphere preparation.

After the solution are prepared, it tested by a general microscope shown in figure 4.13. The resolution test target image in figure 4.14 is captured to measure the size of microspheres.

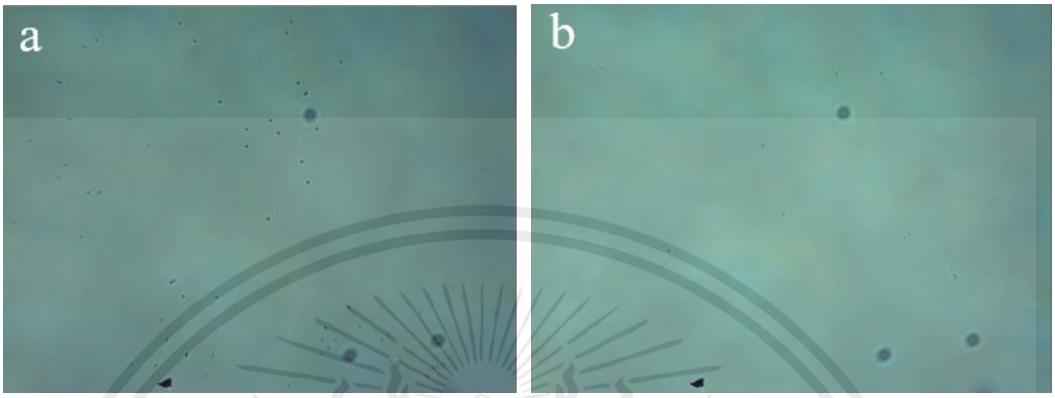

Figure 4.13 Microspheres images for general microscope. (a) Image from general microscope 40x objective lens with 10% of FITC labeled microsphere (b) Image from general microscope 40x objective lens with 1% of FITC labeled microsphere

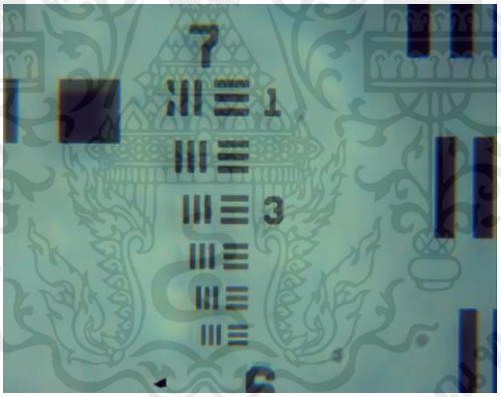

Figure 4.14 The resolution test target image from the 40x microscope.

Thus, the bead size can be calculated by using image in figure 4.13b and image from figure 4.14. ImageJ software is used to calculate FOV and resolution, so the result of 1 bead is 1.36 um. After we use a general microscope observe the FITC labeled microsphere and resolution test target then we observe by using fiber optic fluorescence endomicroscope system to capture the image shown in figure 4.15.

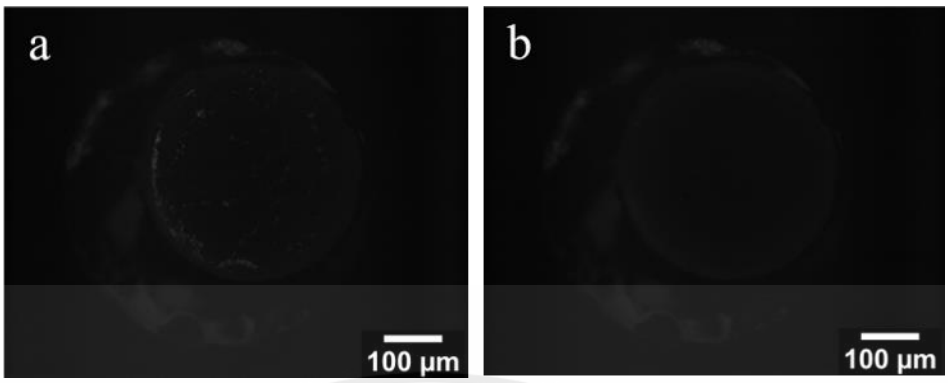

Figure 4.15 Images from the fiber optic fluorescence endomicroscope system. (a) Image from Fiber Optic Fluorescence Endomicroscope system with 10% of FITC labeled microsphere (b) Image from Fiber Optic Fluorescence Endomicroscope system with 1% of FITC labeled microsphere.

Thus, the bead size can be calculated using image in figure 4.15b and image from figure 4.11b. ImageJ software is used to calculate FOV and resolution so the result of 1 bead from fiber bundle is 1.35 um. The cross-section profile of a microsphere shows the FWHM of this microsphere is approximately 1.4 um.

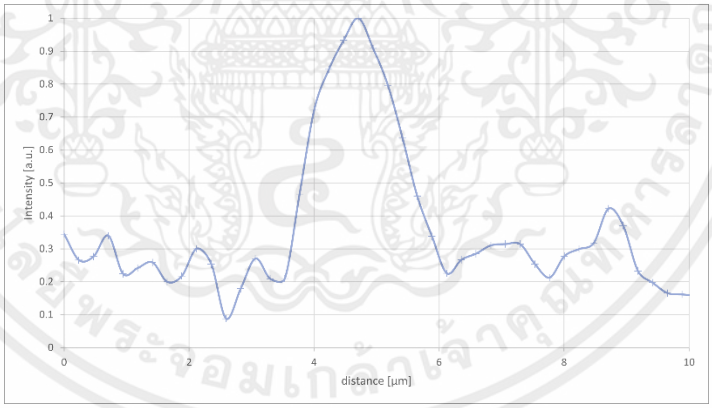

Figure 4.16 A microsphere cross section profile.

Fluorophore of 0.1% concentration and 0.01% concentration dropped on napkins are prepared by drop of dissolved fluorophore on a piece of napkin shown in figure 4.17. The fluorophore dissolve by using acetone solution (1 mg/mL). The fluorophore dropped on a napkin tested by fluorescence endomicroscope system shown in figure 4.18.

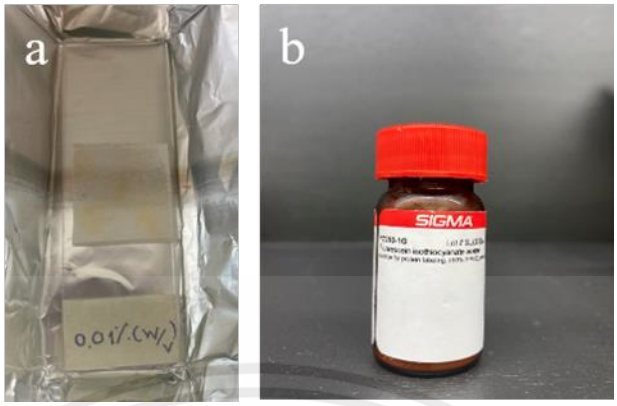

Figure 4.17 FITC stained napkins.

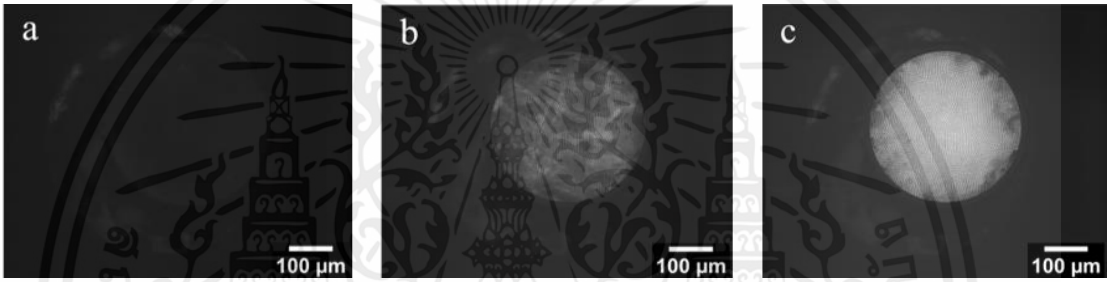

Figure 4.18 FITC stained napkins results. (a) no fluorophore, (b) 0.01%(w/v) of fluorophore, and (c) 0.1%(w/v) of fluorophore.

4.5.3 Fiber optic fluorescence endomicroscope system testing with fluorophore that stained on small piece of pig's intestine.

The small piece of pig's intestine is stained by 0.1% (w/v) FITC on top of the surface, then testing by Fluorescence endomicroscope system results shown in figure 4.19.

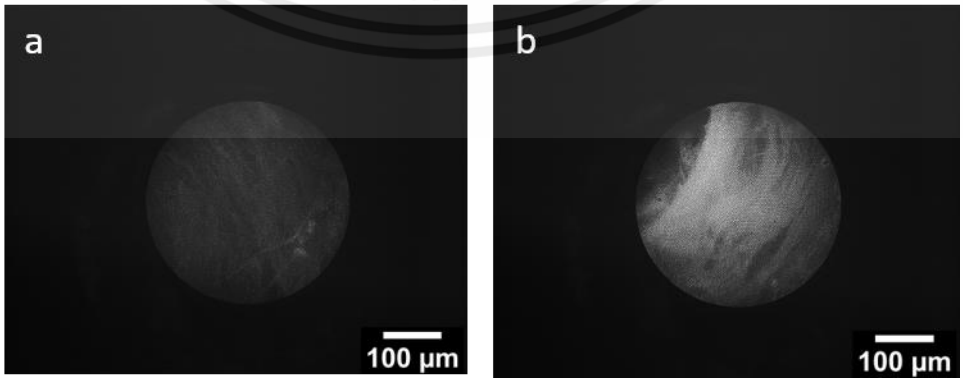

Figure 4.19 The fluorescence image results from intestine tissue of a pig. (a) Staining fluorophore rarely sticks. (b) Fluorophore is well attached to pig's intestine.

4.5.4 Fiber optic fluorescence endomicroscope system testing with fluorophore that stained on an onion membrane.

The small piece of onion membrane is cut and placed on the microscope slide then drops the fluorophore 0.01% w/v FITC on top the onion membrane then place microscope slide with sample under general microscope to see the structure of onion membrane shown in figure 4.20a and testing by fluorescence endomicroscope system shown in figure 4.20b.

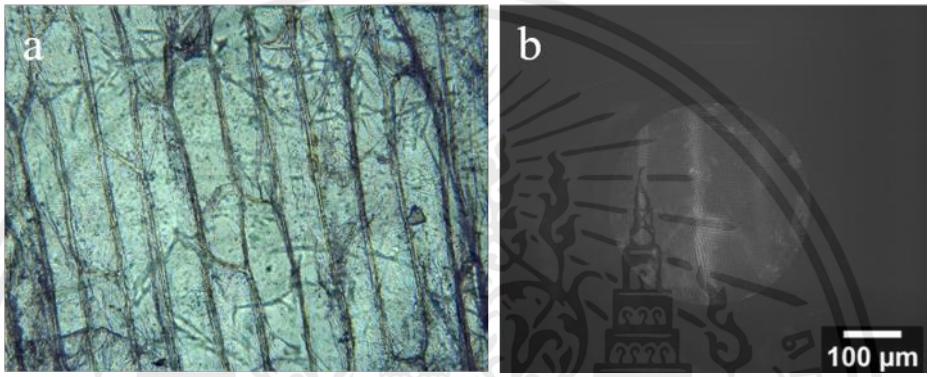

Figure 4.20 FITC stained onion membrane images. (a) Onion cell image result from general microscope. (b) Onion cell image result from fluorescence endoscope system.

4.6 Testing and Evaluation Summary

In section 4.2 results showed that the distance between CCD camera and tube lens is the tube lens focal length, where the error can be neglected because it is only 1% error and when we further test the overall imaging system, the camera can observe the sharp image at the focal plane of the Objective lens. The light source calibration result is that it performs Kohler illumination to fluorescence endomicroscope system. The position of the condenser lens and light source is critical because if it is not Kohler illumination, then the excitation beam will not uniform at the focal plane of the objective lens. In section 4.3 showed the quality of fiber-optic bundle after polishing. This section shows the flatness of both distal end and proximal end of fiber-optic bundle and cleaness of proximal end of fiber bundle. In section 4.4 results show that endomicroscope resolution is up to 3.91 um in non-fluorescence imaging. Additionally, in fluorescence imaging it is able to see the fluorescence microsphere diameter 1 um. The testing described in section 4.4 demonstrates that our fluorescence endomicroscopy

system can enable us to see the cellular imaging in biological samples when stained with compatible fluorophore.

4.7 Software results

This section discusses the result of the GUI and image processing algorithms. Also compare the results of image processing algorithms. Python is used to implement the GUI and image processing algorithms. Image processing results shown in section 4.7.1 and the GUI results shown in section 4.7.2.

4.7.1 Image processing results

In section 3.5 has describes a technique to triangulate source images from list of pixels to artistic images composed of tiles of triangles. After a short theoretical introduction in chapter2, section 2.5.2, now we have applied this technique to a more practical use of FITC stained onion membrane images to get a more efficient image shown in figure 4.22. Also, we have applied a dilation method to enhance the image as described in section 3.5 and the result shown in figure 4.23. Results showed that either interpolation method or dilation method can fill the inter-core spacing of the fiber bundle. Python codes of image dilation and Delaunay triangulation are provide in Appendix A and Appendix B, respectively.

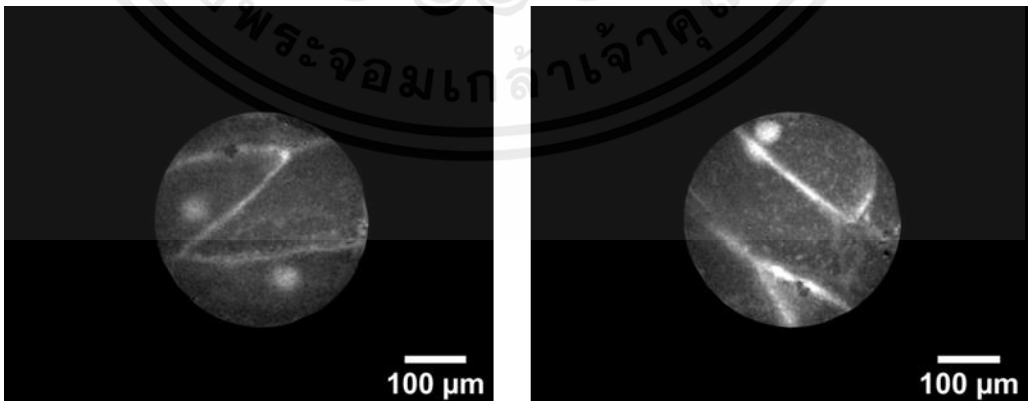

Figure 4.21 The original onion cell images.

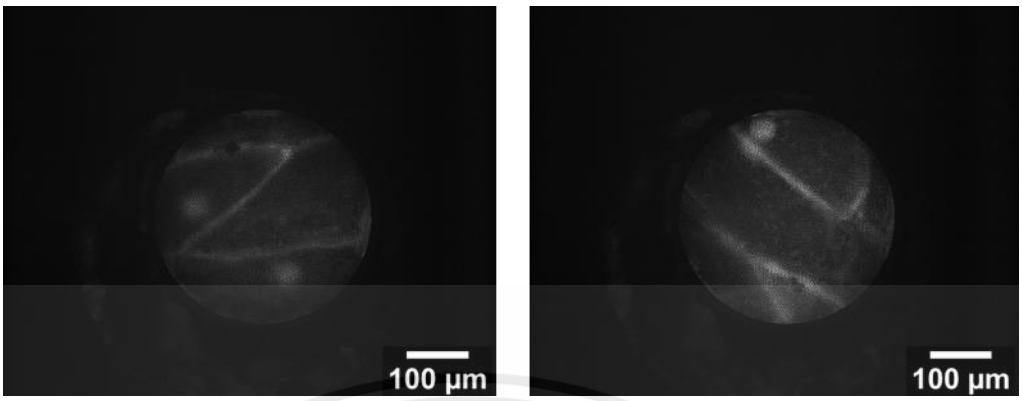

Figure 4.22 Delaunay triangulation interpolation results.

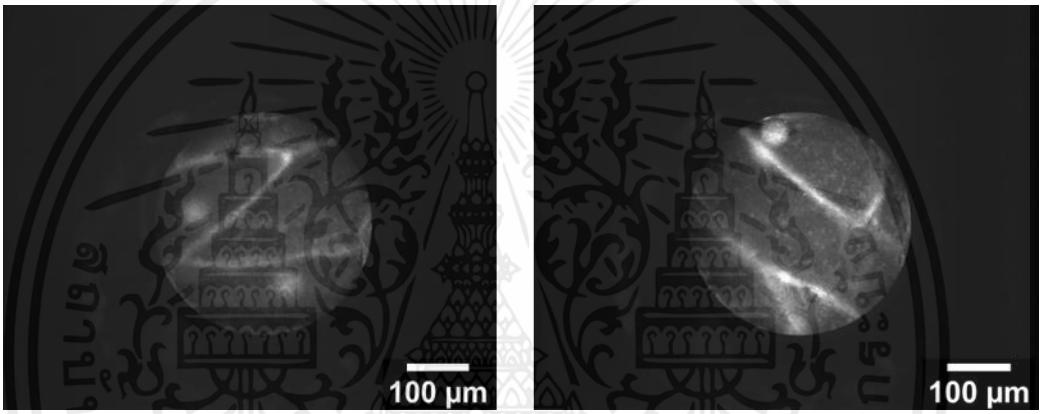

Figure 4.23 Image dilation results.

Delaunay triangulation interpolation method and dilation method are used to fill the inter-core spacing of the fiber bundle with different approaches. Delaunay triangulation interpolation fills the inter-core spacing by interpolate intensity values of every fiber optics cores of the fiber bundle. In contrast, the dilation method fills the inter-core spacing by finding local minima by convolution kernel. The main differences between these two approaches are image results pattern and the speed. Image results pattern in the dilation method still remains the inter-core spacing, but the size of it becomes smaller by morphological operation. The speed of the dilation method depends on the size of the kernel, number of iterations, and the size of the image. When the size of the kernel is square of 5 pixels on each side, number of iterations is 2, and the size of image is 9.1 megapixels, it requires 15 ms for operation. Image results pattern in the Delaunay triangulation interpolation method completely removes the inter-core spacing by filling the inter-core spacing by curve fitted values. The speed of the Delaunay triangulation interpolation method depends on the number of elements inside a fiber

bundle, the size of the image. When the number of elements inside a fiber bundle is 10,000elements, and the size of the image is 9.1 megapixels, it requires 700 ms for operation. The interpolated image quality depends on the accuracy and precision of the reference image used to localization fiber optics cores of the fiber bundle.

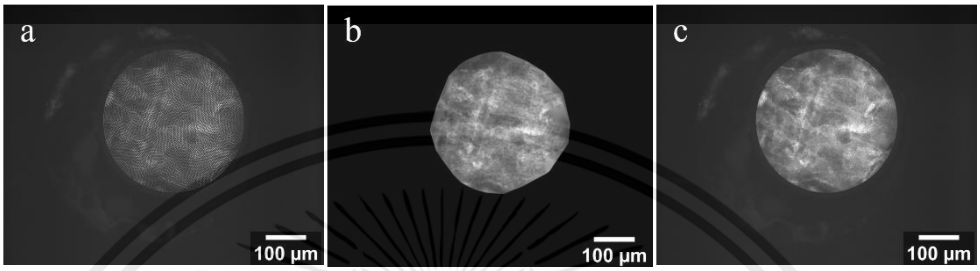

Figure 4.24 Comparison between Delaunay triangulation interpolation and dilation of the fluorophore that is stained on a tissue paper. (a) Original image (b) Delaunay triangulation interpolated image. (c) Dilated image.

Figure 4.25 Comparison between Delaunay triangulation interpolation and dilation of the negative resolution test target, group 6. (a) Original image (b) Delaunay triangulation interpolated image. (c) Dilated image.

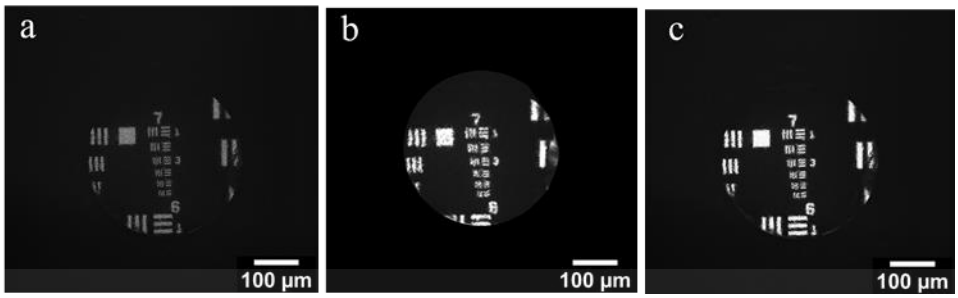

Figure 4.26 Comparison between Delaunay triangulation interpolation and dilation of the negative resolution test target, group 7. (a) Original image (b) Delaunay triangulation interpolated image. (c) Dilated image.

Figure 4.27 shows the comparison of line profiles of group 7 element 1 of USAF 1951 resolution test target. The result shows that image processing methods change the pattern of line profiles when compared with a raw image. Image processing provides continuity between fiber optics cores of the fiber bundle. The dilation method graph is close to the pattern of step function joining together. In contrast, the interpolation method graph is close to the pattern of linear function joining together.

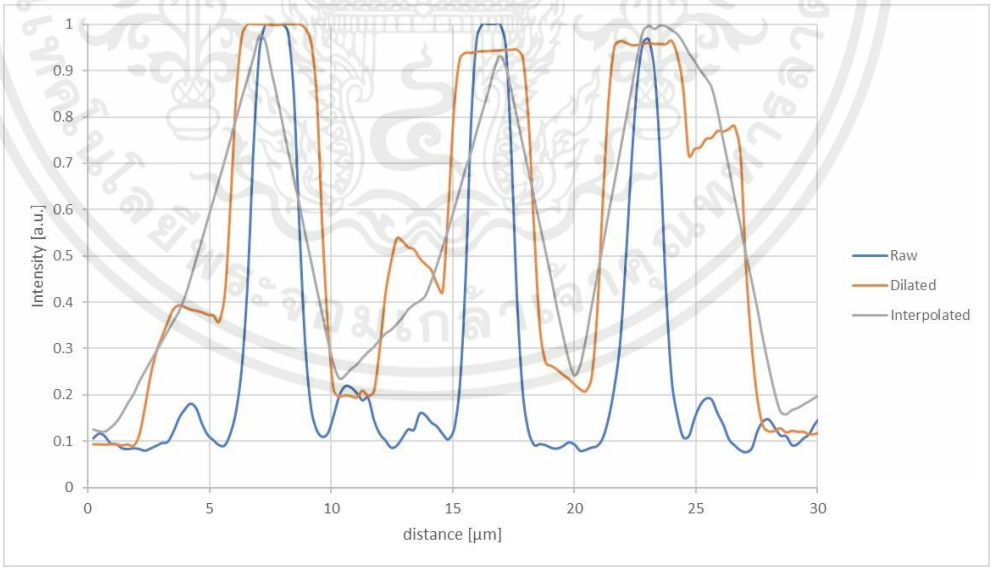

Figure 4.27 Line profiles of USAF resolution test target group 7 element 1.

4.7.2 GUI

In this section, describe the development of a GUI for use with our system. Our software development consists of 2 main windows. First is the login window and second is the camera window. The login window has the purpose to create a folder of patients to store an image which has 3 main parameters. All three parameters consist of the patient ID, name, surname that the user needs to fill it shown in figure 4.28. The python code of GUI is providing in Appendix C.

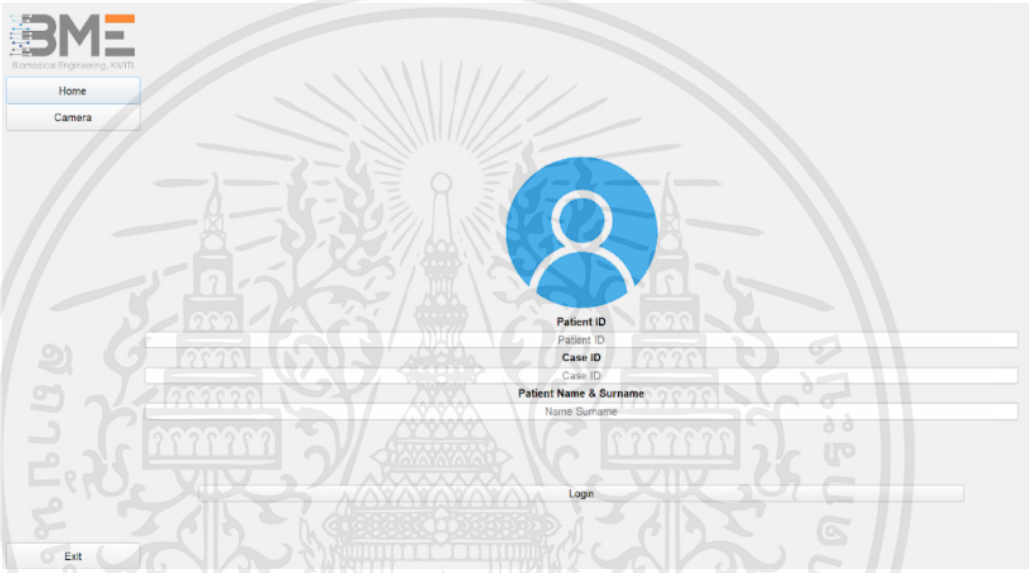

Figure 4.28 Login interface.

After input data of the patient is filled, next is click login. The software will create a directory according to user inputs to save the image as shown in figure 4.29 and a user will be in the page of capture mode which consists of 3 modes. First mode is normal mode which shows a normal image or the real image without any image enhancement as shown in figure 4.30. Second mode is dilation mode as shown in figure 4.31. Third mode is interpolation mode as shown in figure 4.32. When user have captured the image, images going to save in the folder that was already created on the preview page as shown in figure 4.33.

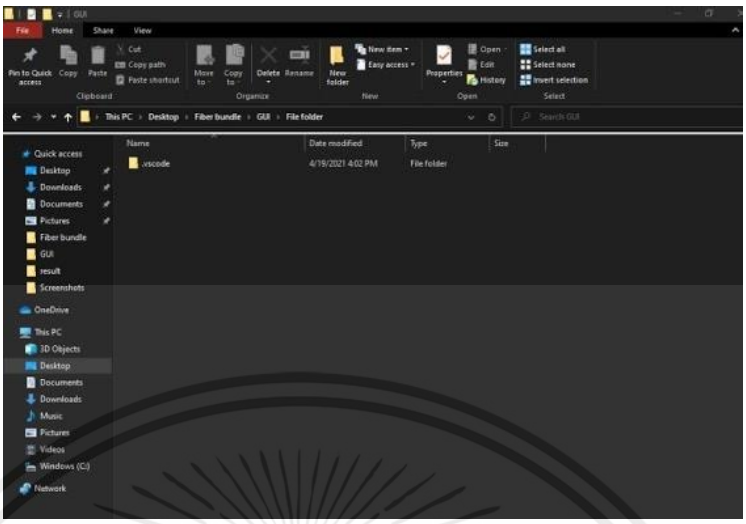

Figure 4.29 Create a directory to save the image.

Figure 4.30 Camera interface in a normal mode.

Figure 4.31 Camera interface in a dilation mode.

Figure 4.32 Camera interface in an interpolation mode.

Figure 4.33 Image saved to the directory that was already created on the previous page.

CHAPTER 5
DISCUSSION AND CONCLUSION

5.1 Introduction

Based on the results obtained in chapter 4, the discussion of the results presented in this chapter. The results from the FOE system are used to discuss whether the objective has been met or not. Finally, the study was discussed based on theoretical, methodological, and experimental approaches followed by suggestions for future research.

5.2 Discussion and suggestion

In this project, there are many methods that have done to aim our objective and get perfect result. In this section, there will be discuss by separating our project into two parts. First part will talk about optical alignment or hardware and how many methods that aim until it works. Second part will talk about software development including GUI and image processing methods.

5.2.1 Optical alignment

First summarize that optical alignment is very difficult to make it align because when you suddenly move or touch it, the system was misaligned. And also, the tolerance of optomechanical components is very significant in the endomicroscope system. A Right-Angle Kinematic Mirror is added between the tube lens and CCD camera sensor in order to provide a degree of freedom to the imaging part for maintaining the image of the fiber bundle to be located on the center of CCD camera sensor. In the illumination part, critical illumination is not suitable for a widefield endomicroscope because the excitation beam is not projected uniformly to the proximal end of the fiber bundle. In contrast, Köhler illumination is suitable for widefield endomicroscope because it projects uniform excitation beams to the proximal end of the fiber bundle. In a flexible fiber bundle endomicroscope, fiber cores use to relay the image from a sample at the distal end of the fiber bundle to the proximal end of the fiber bundle, where the image can further record by imaging sensors. Each fiber core

in the fiber bundle is arranged in a coherent manner that makes the position of each fiber within the bundle remain the same throughout the length of the bundle. With this configuration, image elements are transmitted from one end of the bundle to the other end with the same alignment. The number of pixels in the image is determined by the number of fiber cores contained in the bundle. For example, the Fujikura FIGH-10-350S is 350 μm in diameter and contains 10,000 fiber cores. Smaller bundles are available with lower pixel density because the number of cores is smaller. In addition, the main difference between the fiber bundle imager and an array of individual normal optical fibers is that every fiber core in a fiber bundle imager shares a common cladding instead of having a separate cladding region. A fiber bundle has a relatively higher numerical aperture (NA) or index contrast because it tightly confines the light and reduces the inter-core crosstalk. The crosstalk between fiber core minimizes by keeping inter-core spacing larger than the diameter of fiber cores. Furthermore, the bundle strength is enhanced by wrapping fiber cores with a tough resin buffer layer. The dead space between adjacent cores reduces the light transmission efficiency and creates a pixelated or honeycomb structure in the image. Degrading image resolution by a different method such as image morphology, image filtering, and image interpolation can remove honeycomb artifacts of a fiber bundle. Furthermore, a personal computer is required to perform all computations and to remove this artifact in real-time making it better image quality for medical personnel. From the aforementioned, we proposed the development of FOE with build-in image processing methods to eliminate a pixelation artifact or a honeycomb structure from FOE in which this elimination increase the image quality of captured images by removing unnecessary pixel contents by either dilation or interpolation. Camera parameters can be adjusted to improve the image quality either image contrast or signal to noise ratio of the image.

5.2.2 Optical fiber polishing and cleaving

Polishing the fiber or ferrule end faces of a fiber-optic connector critically influences optical performance and is highly susceptible to error. Yet the polishing process is neither difficult nor mysterious. Other steps in the connector termination procedure, such as crimping, involve mechanically securing the fiber in the connector.

As the final step, polishing prepares the fiber optically to ensure that defects and nonuniformities in the fiber/ferrule end faces of geometry do not degrade the passage of light across the connector joint. The compatibility of fiber bundle and bore diameter of fiber connector is important fiber bundle centering on connector. In this project the fiber bundle is offset from the center of the connector bore because the bore size is a little bit too big for FIGH-10-350S.

An alternative cleaving method, typically used to remove unnecessary fiber from the fiber connector before polishing, by scribe the surplus fiber. The scribe has a hard, sharp tip, generally carbide or diamond, that is used to scratch the tensioned fiber the surplus fiber can be removed from a fiber connector easily. Since both the scribing and breaking process are under manual control, this method is less predictable compared to a good cleaver but can produce sufficient results for polishing. It just needs to ensure that the fiber breaks before a connector ferrules to ensure that the fiber does not has damage before polishing then it can be polished properly. A cleaved fiber surface should be flat and perpendicular to the optic axis.

5.2.3 Software part

The GUI can function properly without error during operation. It can systematically save images of each patient and each case. This helps researchers to distinguish images of each case in future. Image processing algorithms also enhance the image quality by different approaches. Delaunay triangulation interpolation method gives a smoother image, but it uses a long time for operation time. In contrast, dilation method significantly reduces the inter-core spacing size of an image. In addition, the dilation method requires only a short time for operation. Software can further develop algorithms to improve the image contrast such as histogram equalization.

5.3 Conclusion

This research aimed to create an optical fluorescence endomicroscopy system for cervical cancer screening and demonstrated an optical fluorescence endomicroscope by testing with biological cells. FITC is used as fluorescein with LED illumination and fluorescence filters set are compatible with fluorescein to imaging with a high signal-to-noise ratio and specificity for FITC imaging probe. The custom graphical user

interface software is used to perform both data acquisition and pre-processed data images to improve the image quality.

The FOV and resolution of the FOE system are 325 μm in diameter and 3.91 um, respectively. Parameters represent when used a 20X objective lens with 325 μm image circle diameter and 10,000 elements fiber bundle. Both parameters are slightly lower than the capability of the fluorescence microscope because both parameters in FOE are limited by the fiber bundle. The smaller fiber bundle has more flexibility and capability to passed through narrower organs, but the trade-off is the FOV is smaller as the fiber bundle smaller. The software can use to control the camera and enhance the image quality, but it can be further improving by camera parameters control function and more image processing to improve image quality.

This thesis will focus on development of fluorescence endomicroscope with cellular resolution which can further test with FITC labeled peptide to perform diagnostically relevant cervical cancer, thereby reducing the number of invasive, time consuming, and expensive re-operations. This thesis will also serve as an important base for researchers considering this or similar problems for developing and assisting our country.

REFERENCES

[1] Arbyn, M., et al., Estimates of incidence and mortality of cervical cancer in 2018: a worldwide analysis. The Lancet Global Health, 2020. 8(2): p. e191-e203Basu, S., R. S. Gajulapalli, and D. Ghosh. 2008. Implementing tabu search to exploit sparsity in ATSP instances (Report, W.P. No. 2008-10-02 Indian Institute of Management).

[2] Sankaranarayanan, R., et al., A critical assessment of screening methods for cervical neoplasia. International Journal of Gynecology & Obstetrics, 2005. 89: p. S4-S12.

[3] Pierce, M., D. Yu, and R. Richards-Kortum, High-resolution fiber-optic microendoscopy for in situ cellular imaging. JoVE (Journal of Visualized Experiments), 2011(47): p. e2306.

[4] Miller, S.J., et al., In vivo fluorescence-based endoscopic detection of colon dysplasia in the mouse using a novel peptide probe. PloS one, 2011. 6(3).

[5] Bhatla N, et al. Revised FIGO staging for carcinoma of the cervix uteri. Int J Gynecol Obstet 2019; 1–7.

[6] Siegel RL, Miller KD, Jemal A. Cancer statistics, 2020. CA Cancer J Clin. 2020;70:7-30.

[7] National Cancer Institute. Physician Data Query (PDQ). Cervical Cancer Prevention–Patient Version. 2019. Available: https://www.cancer.gov/types/cervical/patient/cervicalprevention-pdq. Updated March 8, 2019. Accessed on November 1, 2019.

[8] Goldie SJ, Gaffikin L, Goldhaber-Fiebert JD, Gordillo-Tobar A, Levin C, et al. (2005) Cost-effectiveness of cervical-cancer screening in five developing countries. N Engl J Med 353: 2158–2168.

[9] Sankaranarayanan R, Basu P, Wesley RS, Mahe C, Keita N, et al. (2004) Accuracy of visual screening for cervical neoplasia: Results from an IARC multicentre study in India and Africa. Int J Cancer 110: 907–913.

[10] Sankaranarayanan R, Nessa A, Esmy PO, Dangou JM (2012) Visual inspection methods for cervical cancer prevention. Best Pract Res Clin Obstet Gynaecol 26: 221–232.

[11] Rubbo SD (1947) The influence of chemical constitution on toxicity; a general survey of the acridine series. Br J Exp Pathol 28: 1–11.

[12] Russell DS, Falconer MA (1941) Antiseptics in brain wounds an experimental study of the histological reaction of cerebral tissues to various antiseptic solutions. British Journal of Surgery 28: 472–499.

[13] Thekkek N, Richards-Kortum R (2008) Optical imaging for cervical cancer detection: solutions for a continuing global problem. Nat Rev Cancer 8: 725–731.

[14] Muldoon TJ, Roblyer D, Williams MD, Stepanek VM, Richards-Kortum R, et al. (2012) Noninvasive imaging of oral neoplasia with a high-resolution fiberoptic microendoscope. Head Neck 34: 305–312.

[15] Vila PM, Thekkek N, Richards-Kortum R, Anandasabapathy S (2011) Use of in vivo real-time optical imaging for esophageal neoplasia. Mt Sinai J Med 78: 894–904.

[16] Pierce MC, Schwarz RA, Bhattar VS, Mondrik S, Williams MD, et al. (2012) Accuracy of In Vivo Multimodal Optical Imaging for Detection of Oral Neoplasia. Cancer Prev Res (Phila)

[17] C. L. Hoy, N. J. Durr, P. Chen, W. Piyawattanametha, H. Ra, O. Solgaard, and A. Ben-Yakar, "Miniaturized probe for femtosecond laser microsurgery and two-photon imaging," Optics Express, Vol. 16 (2008), Issue 13, pp. 9996-10005.

[18] H. Ra, W. Piyawattanametha, M. J. Mandella, P. L. Hsiung, J. Hardy, T. D. Wang, C. H. Contag, G. S. Kino, and O. Solgaard, "Three-dimensional in vivo imaging by a handheld dual-axes confocal microscope," Optics Express, Vol. 16(2008), Issue 10, pp. 7224-7232.

[19] S. Harald and W. Piyawattanametha, "Silicon-based MOEMS and their applications," JOURNAL OF MICRONANOLITHOGRAPHY MEMS AND MOEMS Volume: 7 Issue: 2 Article Number: 020901 DOI:10.1117/1.2913329 Published: APR-JUN 2008.

[20] H. Ra, W. Piyawattanametha, Y. Taguchi, D. Lee, M. J. Mandella, G. S. Kino, C. H. Contag, and O. Solgaard, "Twodimensional MEMS scanner for dual-axes confocal microscopy," IEEE Journal of Micro Electromechanical Systems(JMEMS), Vol. 16, August 2007, pp. 969-976.

[21] A. D. Aguirre, P. R. Herz, Y. Chen, J. G. Fujimoto, W. Piyawattanametha, L. Fan, and M. C. Wu, “Two-axis MEMS Scanning Catheter for Ultrahigh Resolution Three-dimensional and En Face Imaging,” Optics Express, Vol. 15 (2007),Issue 5, pp. 2445-2453.

[22] E. D. Cocker, B. A. Flusberg, W. Piyawattanametha, J. C. Jung, R. P. J. Baretto, T. H. Ko, H. Ra, D. Lee, O. Solgaard, andM. J. Schnitzer, “Portable forms of fiber-optic one- and two-photon fluorescence microendoscopy towards imaging in freely moving mice,” Biophys. J., 154A-154A (2007)

[23] J. T. C. Liu, M. J. Mandella, H. Ra, L. K. Wong, P. Hsiung, T. D. Wang, G. S. Kino, W. Piyawattanametha, C. H. Contag,and O. Solgaard, “A miniature near-infrared dual-axes confocal microscope utilizing a two-dimensional MEMS scanner,”Optics Letters: Vol. 32 (2006), Issue 3, pp. 256-258.

[24] W. Piyawattanametha, R. P. J. Barretto, T. H. Ko, B. A. Flusberg, E. D. Cocker, H. Ra, D. Lee, O. Solgaard, and M. J.Schnitzer, “Fast-scanning two-photon fluorescence imaging based on a microelectromechanical systems two-dimensional scanning mirror,” Optics Letters, Vol. 31, No. 12, July 1, 2006, pp. 2018-2020.

[25] Elizabeth T. H. Fontham, MPH, DrPH1. Cervical Cancer Screening for Individuals at Average Risk: 2020 Guideline Update from the American Cancer Society VOLUME 70, NUMBER 5, SEPTEMBER/OCTOBER 2020

[26] Fontham, ETH, Wolf, AMD, Church, TR, et al. Cervical Cancer Screening for Individuals at Average Risk: 2020 Guideline Update from the American Cancer Society. CA Cancer J Clin. 2020. https://doi.org/10.3322/caac.21628.

[27] Sanderson MJ, Smith I, Parker I, Bootman MD. Fluorescence microscopy. Cold Spring Harb Protoc. 2014;2014(10):pdb.top071795. Published 2014 Oct 1. doi:10.1101/pdb.top071795.

[28] Ghodsi Mohammadi Ziarani, Razieh Moradi, Negar Lashgari, Hendrik G. Kruger, Chapter 10 - Fluorescein Dyes, Editor(s): Ghodsi Mohammadi Ziarani, Razieh Moradi, Negar Lashgari, Hendrik G. Kruger, Metal-Free Synthetic Organic Dyes, Elsevier, 2018, Pages 165-170, ISBN 9780128156476. doi.org/10.1016/B978-0-12-815647-6.00010-8.

[29] ThermoFisher Sciencetific, Fluorescence SpectraViewer.

Available:https://www.thermofisher.com/th/en/home/life-science/cell-analysis/labeling-chemistry/fluorescence-spectraviewer.html#!/

[30] Nguyen, Q., Tsien, R. Fluorescence-guided surgery with live molecular navigation — a new cutting edge. Nat Rev Cancer 13, 653–662 (2013). https://doi.org/10.1038/nrc3566

[31] Robert A. Fry and Anne T. Vinnicombe, Fundamentals of Optics, Fourth Edition.

[32] Murphy, Douglas B. Fundamentals of light microscopy and electronic imaging.

[33] "Optical Filters: Edmund Optics," Edmund Optics Worldwide. [Online]. Available: https://www.edmundoptics.com/knowledge-center/application-notes/optics/optical-filters/. [Accessed: 22-Nov-2020].

[34] M. Bass, "Optical Fibers and Fiber-Optic Communications," in Handbook of optics, 2nd ed., vol. 2, New York: McGraw Hill, 1995.

[35] S. C. Chapra, Applied numerical methods with MATLAB for engineers and scientists. New York: McGraw-Hill, 2012.

[36] University of Tartu, Introduction to image processing. Available: https://sisu.ut.ee/imageprocessing/book/1

[37] Fundamentals of image contours. Available: https://evergreenllc2020.medium.com/fundamentals-of-image-contours-3598a9bcc595

[38] Xin-Yi Gong, Hu Su, De Xu, Zheng-Tao Zhang, Fei Shen, Hua-Bin Yang. An Overview of Contour Detection Approaches[J]. International Journal of Automation and Computing, 2018, 15(6): 656-672

[39] Lee, D.T., Schachter, B.J. Two algorithms for constructing a Delaunay triangulation. International Journal of Computer and Information Sciences 9, 219–242 (1980). Available: https://doi.org/10.1007/BF00977785

[40] Jennifer Gillenwater, J. Ryan Stinnett, Delaunay Triangulation for Image Processing, Elica Skorcheva. Rice University ELEC 301, Sep 27, 2007.

[41] Wiki,GMS:Clough-Tocher, 20 September 2017. Available: https://www.xmswiki.com/wiki/GMS:Clough-Tocher

[42] D. Shin, M. C. Pierce, A. M. Gillenwater, M. D. Williams, and R. R. Richards-Kortum, "A Fiber-Optic Fluorescence Microscope Using a Consumer-Grade Digital Camera for In Vivo Cellular Imaging," PLoS ONE, vol. 5, no. 6, 2010.

[43] H. K. Raut, V. A. Ganesh, A. S. Nair, and S. Ramakrishna, “Anti-reflective coatings: A critical, in-depth review,” Energy & Environmental Science, vol. 4, no. 10, p. 3779, 2011.

[44] Olympus, Transmittance/Wavelength. Available: https://www.olympus-ims.com/en/microscope/mpln/#!cms[focus]=cmsContent11372

[45] Green, F.J., Sigma-Aldrich Handbook of Stains, Dyes and Indicators, p. 377 (1990)

[46] “Spectra Viewer,” Thermo Fisher Scientific. [Online]. Available: https://www.thermofisher.com/order/spectra-viewer-gen2?SID=srch-svtool. [Accessed: 22-Nov-2020].

[47] M. Pierce, D. Yu, and R. Richards-Kortum, “High-resolution Fiber-optic Microendoscopy for in situ Cellular Imaging,” Journal of Visualized Experiments, no. 47, 2011.

[48] J. Reichman, “A general discussion of optical filters,” in Handbook of optical filters for fluorescence microscopy, Brattleboro, Vermont: Chroma Technology Corp, 2017.

[49] K. Osenbach, “Filter Orientation,” UV/VIS Bandpass & Laser Line Filters: 340 - 694.3 nm Center Wavelength. [Online]. Available: https://www.thorlabs.com/newgrouppage9.cfm?objectgroup_id=1001. [Accessed: 22-Nov-2020].

[50] THORLABS, FN96A, Guide to Connectorization and Polishing Optical Fibers.

[51] Sellors JW, Sankaranarayanan R (2003) Colposcopy And Treatment Of Cervical Intraepithelial Neoplasia: A Beginner’s Manual: International Agency for Research on Cancer.

[52] Quinn MK, Bubi TC, Pierce MC, Kayembe MK, Ramogola-Masire D, et al. (2012) High-Resolution Microendoscopy for the Detection of Cervical Neoplasia in Low-Resource Settings. PLoS ONE 7(9): e44924. doi:10.1371/journal.pone.0044924

[53] Van Rossum, G., and Drake, F. 2009. . Python 3 Reference Manual. CreateSpace.

[54] Harris, C., Millman, K., Walt, S., Gommers, R., Virtanen, P., Cournapeau, D., Wieser, E., Taylor, J., Berg, S., Smith, N., Kern, R., Picus, M., Hoyer, S., Kerkwijk, M., Brett, M., Haldane, A., Río, J., Wiebe, M., Peterson, P., Gérard-Marchant, P., Sheppard, K., Reddy, T., Weckesser, W., Abbasi, H., Gohlke, C.,

and Oliphant, T. 2020. Array programming with NumPy. Nature, 585, p.357–362.

[55] Bradski, G. 2000. The OpenCV Library. Dr. Dobb's Journal of Software Tools.

[56] Virtanen, P., Gommers, R., Oliphant, M., Reddy, T., Cournapeau, E., Peterson, P., Weckesser, J., Walt, M., Wilson, J., Millman, N., Nelson, A., Jones, R., Larson, E., Carey, ., Feng, Y., Moore, J., Laxalde, D., Perktold, R., Henriksen, I., Quintero, C., Archibald, A., Pedregosa, P., and SciPy 1.0 Contributors 2020. SciPy 1.0: Fundamental Algorithms for Scientific Computing in Python. Nature Methods, 17, p.261–272.

APPENDICES

APPENDIX A

Image dilation python code

```
import numpy as np
import cv2
from matplotlib import pyplot as plt
import time

img_name = 'filepath'
start = time.time()
image = cv2.imread(img_name,0)
kernel = np.ones((5,5),np.uint8)
dilated = cv2.dilate(image,kernel,iterations = 2)
end = time.time()
print("Elapsed (with compilation) = %s" % (end - start))
plt.imshow(dilated, cmap='gray')
plt.show()
```

APPENDIX B

Image Delaunay triangulation interpolation python code

```
import numpy as np
import cv2
from matplotlib import pyplot as plt
from scipy.interpolate import LinearNDInterpolator
from scipy.interpolate import CloughTocher2DInterpolator
from scipy.interpolate import NearestNDInterpolator
from scipy.interpolate import griddata
from scipy.spatial import Delaunay
import csv
import imutils
import time

filepath1 = 'Reference image'
filepath2 = 'Image'
image = cv2.imread(filepath1)
image2 = cv2.imread(filepath2,cv2.IMREAD_UNCHANGED)
gray = cv2.cvtColor(image, cv2.COLOR_BGR2GRAY)
image2 = cv2.cvtColor(image2, cv2.COLOR_BGR2GRAY)
blurred = cv2.GaussianBlur(gray, (3, 3), 0)
ret, thresh = cv2.threshold(blurred, 220, 255, cv2.THRESH_BINARY)
cnts = cv2.findContours(thresh.copy(), cv2.RETR_EXTERNAL,
    cv2.CHAIN_APPROX_NONE)
cnts = imutils.grab_contours(cnts)
points = []
values = []
X = []
Y = []
for c in cnts:
    # compute the center of the contour
    (x,y),radius = cv2.minEnclosingCircle(c)
    points.append((int(y),int(x)))
grid_x, grid_y = np.mgrid[0:2704:2704j, 0:3376:3376j]
start = time.time()
pointss = [coordinate for coordinate in points]
values = [image2[coordinate] for coordinate in points]
grid_z0 = griddata(pointss, values, (grid_x, grid_y), method='linear')
img = grid_z0.astype(np.uint8)
end = time.time()
print("Elapsed (with compilation) = %s" % (end - start))
plt.imshow(img,cmap='gray')
plt.show()
```

APPENDIX C

GUI application python code

```
import sys
import csv
from PyQt5.QtCore import *
from PyQt5.QtGui import *
from PyQt5.QtWidgets import *
import sys
import cv2
import numpy as np
import os
import datetime
import errno
import imutils
from scipy.interpolate import LinearNDInterpolator
from scipy.interpolate import CloughTocher2DInterpolator
from scipy.interpolate import NearestNDInterpolator
from scipy.interpolate import griddata
from scipy.spatial import Delaunay
import timeit
from time import sleep
import EasyPySpin

class Mainwindow(QDialog):
    class VideoThread1(QThread):
        change_pixmap_signal = pyqtSignal(np.ndarray)
        def __init__(self, myvar, parent=None):
            QThread.__init__(self, parent)
            self.camera = myvar

        def run(self):
                # capture from web cam
                while True:
                    ret, cv_img = self.camera.read()
                    if ret:
                        self.change_pixmap_signal.emit(cv_img)

    class VideoThread2(QThread):
        change_pixmap_signal = pyqtSignal(np.ndarray)
        def __init__(self, myvar, parent=None):
            QThread.__init__(self, parent)
            self.camera = myvar
            self.kernel = np.ones((3,3),np.uint8)
            self.camera = myvar
```

```
        def run(self):
                # capture from web cam
                while True:
                    ret, cv_img = self.camera.read()
                    if ret:
                        gray = cv2.cvtColor(cv_img, cv2.COLOR_BGR2GRAY)
                        blurred = cv2.medianBlur(gray, 7)
                        dilated = cv2.dilate(blurred,self.kernel,iterat
ions = 3)
                        c_dilated = cv2.cvtColor(dilated, cv2.COLOR_RGB
A2BGR)
                        self.change_pixmap_signal.emit(c_dilated)

    class VideoThread3(QThread):
        change_pixmap_signal = pyqtSignal(np.ndarray)
        def __init__(self, myvar, myvar2, parent=None):
            QThread.__init__(self, parent)
            self.camera = myvar
            self.points = myvar2
            self.list = myvar2
            self.i = 0
            self.YY = 2704
            self.XX = 3376
            self.YYY = np.linspace(0, self.YY, self.YY)
            self.XXX = np.linspace(0, self.XX, self.XX)
            self.XXX, self.YYY = np.meshgrid(self.XXX, self.YYY)
            self.Z = np.zeros((self.YY, self.XX),np.uint8)
            self.grid_x, self.grid_y = np.mgrid[0:2704:2704j, 0:3376:33
76j]
            #self.list = []
            self.kernel = np.ones((3,3),np.uint8)
            self.camera = myvar

        def run(self):
                # capture from web cam
                while True:
                    start = timeit.default_timer()
                    ret, cv_img = self.camera.read()
                    if ret:
                        self.image = cv2.dilate(cv_img,self.kernel,iter
ations = 3)
                        self.pointss = []
                        self.values = []
                        gray = cv2.cvtColor(self.image, cv2.COLOR_BGR2G
RAY)
```

```
                        self.values = [gray[coordinate] for coordinate
in self.list]
                        self.pointss = [coordinate for coordinate in se
lf.list]
                        #tri = Delaunay(self.pointss)
                        #func = CloughTocher2DInterpolator(tri, self.va
lues) # 1 ms
                        #self.Z = func(self.YYY, self.XXX)
                        #self.grid_x, self.grid_y = np.mgrid[0:2704:270
4j, 0:3376:3376j]
                        grid_z0 = griddata(self.list, self.values, (sel
f.grid_x, self.grid_y), method='cubic')
                        img = grid_z0.astype(np.uint8)
                        c_dilated = cv2.cvtColor(img, cv2.COLOR_GRAY2BG
R)
                        self.change_pixmap_signal.emit(c_dilated)
                        stop = timeit.default_timer()
                        self.pointss = None
                        self.values = None
                        print('Time: ', stop - start)

    def __init__(self):
        super(Mainwindow, self).__init__()
        self.list, self.values = [],[]
        filepath = ''   #Coordinate lists file
        with open(filepath,'r') as csvfile:
            reader = csv.reader(csvfile, delimiter=',')
            for row in reader:
                self.list.append((int(row[0]),int(row[1])))
        self.setFont(QFont('Arial', 15))
        self.list = [(list[0]+30,list[1]+122) for list in self.list]
        self.cap = EasyPySpin.VideoCapture(0)
        self.menubar = QVBoxLayout()
        self.menubar.setContentsMargins(0, 0, 0, 0)
        titles = ['Home', 'Camera', 'Exit']
        frameID = [0, 1, 2]
        buttons = [QPushButton(title) for title in titles]
        tag_titles = ['Patient ID', 'Case ID', 'Name Surname']
        tag_IDs = [0, 1, 2]
        #self.tags = [QLineEdit(tag_title) for tag_title in tag_titles]
        self.tags = [QLineEdit(), QLineEdit(), QLineEdit()]
        for tag_title, n in zip(tag_titles, tag_IDs):
            self.tags[n].setPlaceholderText(tag_title)
        labelImage = QLabel()
        convert_to_Qt_format = QImage('BME_logo.png')
        p = convert_to_Qt_format.scaledToWidth(250)
```

```
        labelImage.setPixmap(QPixmap.fromImage(p))
        labelImage.setAlignment(Qt.AlignHCenter)
        self.menubar.addWidget(labelImage)
        self.button_group = QButtonGroup()
        self.button_group.addButton(buttons[0], frameID[0])
        self.button_group.addButton(buttons[1], frameID[1])
        self.button_group.addButton(buttons[2], frameID[2])
        self.menubar.addWidget(buttons[0])
        self.menubar.addWidget(buttons[1])
        verticalSpacer = QSpacerItem(20, 40, QSizePolicy.Minimum, QSize
Policy.Expanding)
        self.menubar.addItem(verticalSpacer)
        self.menubar.addWidget(buttons[2])
        buttons[0].setCheckable(False)
        buttons[1].setCheckable(False)
        buttons[2].setCheckable(False)
        buttons[0].setMinimumHeight(50)
        buttons[1].setMinimumHeight(50)
        buttons[2].setMinimumHeight(50)

        scale_factor = 0.5625
        width = 1600
        self.path = ''
        self.image_label = QLabel()
        self.image_label.setAlignment(Qt.AlignHCenter)
        self.capturebutton = QPushButton("Capture")
        self.mode_selection = QPushButton("Acquisition Mode")
        self.disply_width = width
        self.display_height = int(width * scale_factor)
        self.image_label.resize(self.disply_width, self.display_height)

        self.capturebutton.setShortcut('c')
        self.mode_selection.setShortcut('a')
        self.stack1 = QWidget()
        self.stack2 = QWidget()

        self.stack1UI()
        self.stack2UI()

        self.Stack = QStackedWidget (self)
        self.Stack.addWidget (self.stack1)
        self.Stack.addWidget (self.stack2)

        hbox = QHBoxLayout(self)
        hbox.addLayout(self.menubar, 12)
        hbox.addWidget(self.Stack, 88)
```

```
        hbox.setSpacing(0)

        self.setLayout(hbox)
        self.button_group.idClicked.connect(self.display)
        buttons[2].clicked.connect(self.closeEvent)
        self.capturebutton.clicked.connect(self.on_click)
        self.mode_selection.clicked.connect(self.choose)
        self.setGeometry(10, 10, 1920, 1080)
        self.setWindowTitle('StackedWidget demo')

        self.thread = [self.VideoThread1(myvar = self.cap), self.VideoT
hread2(myvar = self.cap), self.VideoThread3(myvar = self.cap, myvar2 =
self.list)]

        for i in range(len(self.thread)):
            self.thread[i].change_pixmap_signal.connect(self.update_ima
ge)
            self.thread[i].setTerminationEnabled(True)

        self.kernel = np.ones((5,5),np.uint8)

        self.thread[0].start()
        self.mode_label = ['Normal mode','Dilation mode','Interpolation
 mode']
        self.mode = 1
        self.mode_selection.setText(self.mode_label[self.mode-1])


    def stack1UI(self):
        verticalSpacer = QSpacerItem(20, 40, QSizePolicy.Minimum, QSize
Policy.Expanding)
        layout = QVBoxLayout()
        layout.addItem(verticalSpacer)
        labelImage = QLabel()
        convert_to_Qt_format = QImage('login_logo.png')
        p = convert_to_Qt_format.scaledToWidth(300)
        labelImage.setPixmap(QPixmap.fromImage(p))
        labelImage.setAlignment(Qt.AlignHCenter)
        layout.addWidget(labelImage)
        patient_id_label = [QLabel('Patient ID'), QLabel('Case ID'), QL
abel('Patient Name & Surname')]
        patient_id_label[0].setAlignment(Qt.AlignHCenter)
        patient_id_label[1].setAlignment(Qt.AlignHCenter)
        patient_id_label[2].setAlignment(Qt.AlignHCenter)
        patient_id_label[0].setFont(QFont('Arial', 15, QFont.Bold))
        patient_id_label[1].setFont(QFont('Arial', 15, QFont.Bold))
```

```
        patient_id_label[2].setFont(QFont('Arial', 15, QFont.Bold))
        self.tags[0].setAlignment(Qt.AlignHCenter)
        self.tags[0].setFont(QFont('Arial', 15))

        self.tags[1].setAlignment(Qt.AlignHCenter)
        self.tags[1].setFont(QFont('Arial', 15))

        self.tags[2].setAlignment(Qt.AlignHCenter)
        self.tags[2].setFont(QFont('Arial', 15))

        layout.addWidget(patient_id_label[0])
        layout.addWidget(self.tags[0])
        layout.addWidget(patient_id_label[1])
        layout.addWidget(self.tags[1])
        layout.addWidget(patient_id_label[2])
        layout.addWidget(self.tags[2])
        loginbutton = QPushButton("Login")
        loginlayout = QHBoxLayout()
        horizontalSpacer = QSpacerItem(100, 20, QSizePolicy.Minimum, QS
izePolicy.Expanding)
        loginlayout.addItem(horizontalSpacer)
        loginlayout.addWidget(loginbutton)
        loginlayout.addItem(horizontalSpacer)
        layout.addLayout(loginlayout)
        #self.setTabText(0,"Contact Details")
        self.stack1.setLayout(layout)

        loginbutton.clicked.connect(self.GoToCamera)

    def stack2UI(self):
      layout = QVBoxLayout()
      layout.addWidget(self.image_label)
      layout.addWidget(self.mode_selection)
      layout.addWidget(self.capturebutton)
      self.image_label.setAlignment(Qt.AlignCenter)

      self.stack2.setLayout(layout)
    @pyqtSlot(np.ndarray)
    def update_image(self, cv_img):
        """Updates the image_label with a new opencv image"""
        qt_img = self.convert_cv_qt(self.processingMode(cv_img, 1))
        self.image_label.setPixmap(qt_img)

    def convert_cv_qt(self, cv_img):
        """Convert from an opencv image to QPixmap"""
        rgb_image = cv2.cvtColor(cv_img, cv2.COLOR_BGR2RGB)
```

```
        h, w, ch = rgb_image.shape
        bytes_per_line = ch * w
        convert_to_Qt_format = QImage(rgb_image.data, w, h, bytes_per_l
ine, QImage.Format_RGB888)
        p = convert_to_Qt_format.scaled(self.disply_width, self.display
_height, Qt.KeepAspectRatio)
        return QPixmap.fromImage(p)

    def on_click(self):
        frame1, im1 = self.cap.read()
        self.image = im1

        now = datetime.datetime.now()# dd/mm/YY
        self.d1 = now.strftime("%d_%m_%Y_%H_%M_%S_%f")[:-3]
        for i in range(1,4):
            im = self.processingMode(self.image, i)
            image_name = self.d1+'('+str(i)+').jpg'
            cv2.imwrite(os.path.join(self.path, image_name), im)
        print('CAP')

    def display(self,i):
        if i == 0:
            self.Stack.setCurrentIndex(i)
        elif i == 1:
            self.GoToCamera(i)

    def GoToCamera(self, i):
      self.path = os.getcwd() + '/' + self.tags[0].text() + '_' + self.
tags[2].text() + '/' + self.tags[1].text()
      tags_status = [0, 0, 0]
      for i in range(len(tags_status)):
         tags_status[i] = self.checkTags(self.tags[i])
      if np.all(tags_status):
         try:
            os.makedirs(self.path)
         except OSError as e:
            if e.errno != errno.EEXIST:
               raise print('Patient record is alrady exist')
         self.Stack.setCurrentIndex(1)
      else:
         warning_text = ''
         warning_texts = ['Please enter patient ID.', 'Please enter cas
e ID.', 'Please enter patient name and surname.']
         msg = QMessageBox()
         msg.setIcon(QMessageBox.Warning)
         msg.setWindowTitle("Invalid input(s)")
```

```
        for i in range(len(tags_status)):
            if tags_status[i] == 0:
                warning_text = warning_text + warning_texts[i] + '\n'
        msg.setText(warning_text)
        msg.exec_()

    def closeEvent(self, event):
        self.cap.release()
        self.close()

    def checkTags(self, a):
        if a.text() == '':
            self.Stack.setCurrentIndex(0)
            return 0
        elif a.text() != '':
            return 1

    def choose(self):
        self.threatControl(self.mode)

    def threatControl(self, mode):
        self.thread[int(mode - 1)].terminate()
        self.thread[int(mode % len(self.thread))].start()
        self.mode = int((mode % len(self.thread)) + 1)
        print(self.mode)
        self.mode_selection.setText(self.mode_label[self.mode-1])

    def processingMode(self, cv_img, imageProcessingMode):
        if imageProcessingMode == 1:
            return cv_img
        elif imageProcessingMode == 2:
            gray = cv2.cvtColor(cv_img, cv2.COLOR_BGR2GRAY)
            blurred = cv2.medianBlur(gray, 7)
            dilated = cv2.dilate(blurred,self.kernel,iterations = 1)
            c_dilated = cv2.cvtColor(dilated, cv2.COLOR_RGBA2BGR)
            return c_dilated
        elif imageProcessingMode == 3:
            start = timeit.default_timer()
            self.pointss = []
            self.values = []
            gray = cv2.cvtColor(cv_img, cv2.COLOR_BGR2GRAY)
            blurred = cv2.medianBlur(gray, 7)
            dilated = cv2.dilate(blurred,self.kernel,iterations = 3)
            self.grid_x, self.grid_y = np.mgrid[0:2704:2704j, 0:3376:33
76j]
```

```
            self.values = [dilated[coordinate] for coordinate in self.l
ist]
            self.pointss = [coordinate for coordinate in self.list]
            grid_z0 = griddata(self.list, self.values, (self.grid_x, se
lf.grid_y), method='cubic')
            img = grid_z0.astype(np.uint8)
            c_dilated = cv2.cvtColor(img, cv2.COLOR_GRAY2BGR)
            stop = timeit.default_timer()
            self.pointss = None
            self.values = None
            print('Time: ', stop - start)
            return c_dilated



def main():
    app = QApplication(sys.argv)
    print(QStyleFactory.keys())
    app.setStyle('Fusion')
    ex = Mainwindow()
    ex.showFullScreen()
    sys.exit(app.exec_())

if __name__ == '__main__':
    main()
```